Properties of type II superconductors studied by the muon spin rotation method

Yu. M. Belousov, V. N. Gorbunov, V. P. Smilga, and V. I. Fesenko

Physicotechnical Institute, Moscow

Usp. Fiz. Nauk **160**, 55–101 (November 1990)

This review presents a systematic account of the theory of the muon spin rotation method of studying type II superconductors. Experimental investigations of the vortex structure and antiferromagnetism in high-T_c superconductors are discussed and analyzed. Theoretical studies show that the parameters of the vortex structure and of the superconductor itself can be determined reliably only by using single crystal samples. Data obtained from polycrystalline samples at present can only provide a qualitative analysis. Theory shows that to obtain the required information with single-crystal high-T_c superconductors it is best to use two orientations of the external magnetic field: along the axis of anisotropy and perpendicular to it. The theory that has been developed makes it possible to analyze the behavior of the spin polarization of the muon and to determine the parameters of the vortex structure, both for an ideal lattice, and in the case of strong pinning. Experimental results of a study of antiferromagnetic states in high-T_c ceramics are analyzed and promising directions of research are pointed out.

INTRODUCTION

Let us recall briefly the ideas behind the muon method. It is based on the nonconservation of parity in the weak interaction. As is well known, the muon, an unstable lepton, decays according to the scheme $\mu^+ \to e^+ + \nu_e + \bar{\nu}_\mu$. The average lifetime is $\tau_\mu = 2.2 \cdot 10^{-6}$ s. It has been shown in the theory of the weak interaction that for the muon at rest the angular distribution of the decay positrons of a given energy is

$$\frac{d\Gamma_\varepsilon(\theta, \varphi)}{\Gamma} = \frac{1}{2\pi}[(3 - 2\varepsilon) - \cos\theta(1 - 2\varepsilon)]\,\varepsilon^2 d\varepsilon d\Omega,$$

and this expression integrated over energy and the angle φ becomes

$$\frac{d\Gamma(\theta)}{\Gamma} = \frac{1}{2}\left(1 + \frac{1}{3}\cos\theta\right) d\cos\theta,$$

where Γ is the total-decay probability. The polar axis is chosen in the direction of the muon spin; correspondingly, θ is the angle between the positron momentum and the spin direction, and, finally, $\varepsilon = E_{e^+}/E_{max}$ is the normalized energy of the positron ($E_{max} \approx 53$ MeV). The decay scheme and the directional diagram are shown in Fig. 1a. It is clear, therefore, that if sufficient statistics is collected it is possible to determine the polarization of the muon $\mathbf{P} = \langle\boldsymbol{\sigma}\rangle$. By distributing the events over small intervals of time of decay (t_i, t_{i+1}), which may be called time channels, one obtains a histogram that describes the function $\mathbf{P}(t)$. The accuracy of the measurements is determined mainly by the collection statistics.

The principle of the muon method is quite simple. An ensemble of muons with polarization $\mathbf{P}(0)$ is injected into the sample, and then the time dependence of the polarization $\mathbf{P}(t)$ is studied. The orthodox procedure that is used is as

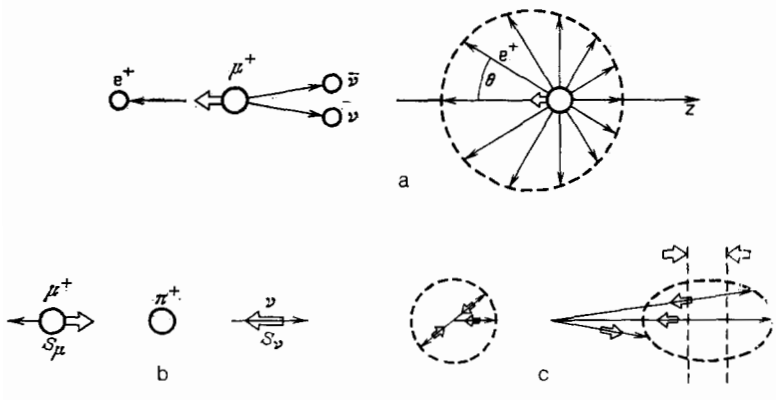

FIG. 1. a) Decay scheme and directional diagram for the decay of a muon into a positron, a neutrino, and an antineutrino. b) Origin of muon polarization in the decay (the thin arrows indicate the momenta and the thick arrows the projections of the spins. c) Direction of the muon spin and momentum in the decay (in the rest system of the pion and in the laboratory system).

 0038-5670/90/110911-27$01.00

follows. The time that the muon enters the sample is recorded ($t_0 = 0$) and the clock is started. Then counters (a positron telescope) are used to detect the time of the decay, t_1. In the time interval $\Delta T = t_1 - t_0$ only a single muon is within the target (if there is more than one muon the event is discarded). After the collection of the statistics (usually 10^6 to 10^8 decays) the histogram is plotted to determine $\mathbf{P}(t)$. In the classical scheme the ensemble of muons is formed as a result of the collection of a number of measurements much larger than the number of single quantum objects.

It is obvious that the behavior of $\langle \sigma(t) \rangle$ is completely determined by the local magnetic field at the location of the muon, including the external field and the internal fields in the material. Since a muon can stop at any point in the sample, the experiment yields the average pattern over the entire target. It should also be mentioned that the initial polarization $\mathbf{P}(0)$ of the muon remains essentially unchanged during the time $t_{th} \sim 10^{-10}$ s it takes to slow down (thermalize). In fact, the angular frequency of precession is $\omega \approx 0.85 \cdot 10^5$ B s^{-1}, and therefore in fields $B \sim 1$–5 kG the angle of rotation in the time t_{th} is $\varphi = \omega t_{th} \leqslant 0.04$ rad.

Beams of polarized muons are produced in proton accelerators. The beam of protons impinges on a meson-forming target, where positive and negative pions with a lifetime of $2.6 \cdot 10^{-8}$ s are created. Magnetic lenses separate out the π^+ beam, which, decaying, forms polarized positive muons. The decay scheme is shown in Figs. 1a and 1b. Then the beam of muons is directed onto the target. For the standard conditions the muon momentum is $p_\mu \approx 10^2$ MeV/c. The range of these muons in matter is $l \approx 10$ g/cm^2 (which for copper is about 1 cm), and for this reason these beams are usually slowed by means of filters (usually graphite) before impinging on the target. In another version the muons that are separated out are those in the muon beam that have come from π^+ that have been trapped on the surface of the meson-forming target. These have a relatively small momentum $p_\mu \sim 29.8$ MeV/c. Their range is about 0.15 g/cm^2 (which is $l \approx 0.017$ cm for copper). Thus, the characteristic thicknesses of the metal targets is varied from 10^{-2} to 0.3–0.5 cm.

The study of superconductors is one of the most effective applications of the μSR (muon spin rotation) method. One can distinguish a hierarchy in the value of the information obtained. In one case we learn the details of the "biography" of a muon in matter (for example "anomalous muonium" in semiconductors). This is very interesting, but the physical interest in problems of this class narrows down to the partial problem—the behavior of atomic hydrogen in this material. In the other case, the one that we believe is the most interesting, the muon method provides information on the properties of the studied object *per se*. It is this version of the method that is involved in the study of superconductors. The conceptual aspect of the muon method reduces, as usual, to the determination of the structure and the distribution of the internal local magnetic fields in the superconductor.

The simplest muon experiment is the study of the intermediate state of a type I superconductor.[1-3] The intermediate state (usually a layered structure with alternating layers of superconducting and normal phase) is found in regions of a material, where, for reasons of geometry, the external field exceeds the critical field. By the muon method it is possible to determine the relative volumes of the two phases in the sample. Assuming that the external magnetic field is directed along the z axis and the initial polarization of the muon is along the x axis, and that the magnetic field is totally excluded from the superconductor, we can write the polarization as

$$P_x(t) = (1 - v) \int \cos(\gamma_\mu h t)\, p(h)\, dh + v,$$
$$P_y(t) = (1 - v) \int \sin(\gamma_\mu h t)\, p(h)\, dh; \tag{I.1}$$

where v is the relative volume of the superconducting phase, $p(h)$ is the density of the magnetic field distribution (the probability of a given field) in the normal phase. The initial polarization is taken to be unity. It can be seen from formula (I.1) that the value of v can be obtained from a measurement of the initial precession amplitude and the conserved polarization component.

By applying the muon method to type II superconductors one can obtain information on the distribution of the microscopic fields within the sample and on the geometry of the Abrikosov vortex structure, and in addition, determine the London penetration depth $\lambda(T)$ and the correlation length $\xi(T)$ of the superconductor. The methods of neutron diffraction and nuclear magnetic resonance as applied to the study of the vortex structure have a number of fundamental limitations. In particular, neutron experiments are hindered by small effective cross sections and are carried out at small scattering angles (the characteristic Bragg angle is $\sim 20'$). This limitation severely degrades the accuracy of the experiments.[4] Because of the skin effect, studies of superconductors by NMR methods are limited to the study of the near-surface layers of the sample.

The use of the muon method for the determination of the characteristics of the vortex lattice in mixed states of type II superconductors was first proposed in Ref. 5. The idea underlying the application of the muon method to the study of type II superconductors is trivial.

Let us consider the behavior of an ensemble of muons in a two-dimensional periodic vortex lattice of a superconductor. We assume that the initial polarization of the ensemble is perpendicular to the magnetic field (the experiment takes place in a transverse field). Henceforth we shall assume that the induction B is directed along the z axis of a Cartesian coordinate system, and the initial polarization is equal to unity and is directed along the x axis. We shall denote the component of the polarization along the x axis as $P(t)$. Taking into account the periodicity of the vortex lattice, we write the time dependence of the polarization as a two-dimensional integral over the unit cell of the lattice:

$$\mathbf{P}(t) = \int \frac{1}{S} \cos(\omega(\boldsymbol{\rho})\, t)\, d\boldsymbol{\rho}, \tag{I.2}$$

where S is the area of the unit cell, $\boldsymbol{\rho}$ is the two-dimensional position vector, and $\omega(\boldsymbol{\rho}) = \gamma_\mu h(\boldsymbol{\rho})$ is the precession frequency of a muon in the microscopic field, $h(\boldsymbol{\rho})$. The Fourier spectrum $P(\omega)$ of the polarization in fact coincides with the distribution density $p(h)$ of the microscopic magnetic field:

$$P(\omega) = \gamma_\mu^{-1} p(h),$$
$$P(\omega) = \int \frac{1}{S} \delta(\omega - \omega(\boldsymbol{\rho}))\, d\boldsymbol{\rho}. \tag{I.3}$$

As is evident, one can thus determine the distribution of the fields in the vortex lattice by means of the muon method. In a number of cases the field distribution can be calculated theoretically within the framework of the Ginsburg–Landau (GL) theory.

Let us also introduce a helpful formula that describes the behavior of the polarization if the mutual orientations of $\mathbf{h}(\rho)$ and $\mathbf{P}(0)$ are arbitrary:

$$P_\alpha(t) = \mu_{\alpha\beta}(t) P_\beta(0); \tag{I.4}$$

where

$$\mu_{\alpha\beta}(t) = \langle n_\alpha n_\beta \rangle + \langle (\delta_{\alpha\beta} - n_\alpha n_\beta) \cos(\omega t) \rangle + e_{\alpha\beta\gamma} \langle n_\gamma \sin(\omega t) \rangle, \tag{I.5}$$

and $n_\alpha = h_\alpha / h$, and the average is taken over the entire ensemble of muons at time t (see e.g., Ref. 3).

For many years the use of the muon method for studying superconductors had not attracted much attention. Active interest in this method was kindled after the discovery of a new class of superconductors—high-temperature (high-T_c) superconductors. (In the Soviet literature the properties of high-T_c superconductors have been examined in detail in Refs. 6–9.) However, the interpretation of the experimental results has so far been quite arbitrary, and the potentialities of the muon method have not been used to their fullest. Below, we shall examine in detail the potentialities of the muon method as applied to type II superconductors and the present state of the problem.

1. THE PRINCIPAL PROPOSITIONS OF THE GINSBURG–LANDAU THEORY

Let us review briefly the principal propositions of the Ginsburg–Landau theory. The free energy of a superconductor is written as[10]

$$F = \int \left[\alpha(t)(T - T_c) |\psi|^2 + \frac{\beta(T)}{2} |\psi|^4 + \frac{1}{4m} \left| \left(-i\hbar \nabla - \frac{2e}{c} \mathbf{A} \right) \psi \right|^2 + \frac{h^2}{8\pi} \right] dV, \tag{1.1}$$

where m is the effective mass, T_c is the critical temperature, h is the microscopic magnetic field, ψ is the order parameter ($\psi = 0$ in the normal phase), and c is the velocity of light. Carrying out variations with respect to $\delta\psi$ and $\delta\mathbf{A}$ we obtain the Ginsburg–Landau equations

$$\alpha(T)(T - T_c)\psi + \beta(T)|\psi|^2\psi + \frac{1}{4m}\left(-i\hbar\nabla - \frac{2e}{c}\mathbf{A}\right)^2 \psi = 0, \tag{1.2a}$$

$$\frac{\operatorname{curl}\mathbf{h}}{4\pi} = \frac{\mathbf{j}}{c} = \frac{e\hbar}{2ic}\frac{1}{m}(\psi^*\nabla\psi - \psi\nabla\psi^*) - \frac{2e^2}{c^2}\frac{1}{m}\mathbf{A}|\psi|^2, \tag{1.2b}$$

to which it is necessary to add the boundary condition

$$\mathbf{n}\left(-i\hbar\nabla - \frac{2e}{c}\mathbf{A}\right)\psi \Big|_b = 0 \tag{1.2c}$$

($\mathbf{n}$ is the normal to the surface), which states that the current that passes through the surface of the sample is zero.

The solution of Eqs. (1.2), $\psi = \psi_0 = [\alpha(T)(T_c - T)/\beta(T)]^{1/2}$ in zero field, $\mathbf{A} = 0$, $\mathbf{h} = 0$ corresponds to the complete Meissner effect; that is, the magnetic field is completely expelled from the interior of the superconductor. With an accuracy to terms of order h in the quantity $|\psi|^2$ in Eq. (1.2b) one can replace ψ_0^2 by the value of $|\psi|^2$ in the absence of a field. Taking the curl of both sides of the equation we obtain the London equation

$$\mathbf{h} + \lambda^2 \operatorname{curl}\operatorname{curl}\mathbf{h} = 0, \tag{1.3}$$

where

$$\lambda(T) = \left(\frac{mc^2}{8\pi e^2 \psi_0^2} \right)^{1/2}$$

is the London penetration depth; this is the characteristic length of screening of the magnetic field by the superconducting currents.

In zero field Eq. (1.2a) takes the form

$$-\xi^2\nabla^2 \frac{\psi}{\psi_0} = \frac{\psi}{\psi_0} - \left|\frac{\psi}{\psi_0}\right|^2 \frac{\psi}{\psi_0}; \tag{1.4}$$

where we have introduced the quantity

$$\xi(t) = \left[\frac{\hbar^2}{4m\alpha(T)(T_c - T)} \right]^{1/2}$$

which is the correlation length, or the characteristic length of variation of the order parameter ψ.

The temperature dependence of the phenomenological parameters $\alpha(T)$ and $\beta(T)$ and, accordingly, $\lambda(T)$ and $\xi(T)$ can be derived from microscopic theory:[11]

$$\xi(T) = \xi(0)\left(1 - \frac{T}{T_c}\right)^{-1/2}, \tag{1.5a}$$

$$\lambda(T) = \lambda(0)\left(1 - \frac{T}{T_c}\right)^{-1/2} \tag{1.5b}$$

The experimental data are usually well described by the empirical formula

$$\lambda(T) = \lambda(0)\left[1 - \left(\frac{T}{T_c}\right)^4\right]^{-1/2} \tag{1.6}$$

It is well known that the value of the Ginsburg–Landau parameter $\varkappa = \lambda(T)/\xi(T)$ has a large effect on the properties of the superconductor.[4,10] For $\varkappa < 1/\sqrt{2}$ we have a type I superconductor with an ideal Meissner effect in fields that are lower than the critical field H_c. For $\varkappa > 1/\sqrt{2}$, we have a type II superconductor. For type II superconductors it is energetically favorable in a broad range of fields ($H_{c1} < H_{ext} < H_{c2}$) to stratify into regions of the normal and the superconducting phase—the so-called mixed state of a superconductor—a two-dimensional regular lattice of vortical filaments. Each of the vortical filaments carries a magnetic flux $\Phi_0 = hc/2e = 2.07 \cdot 10^{-7}$ Oe·cm^2 ($h = 2\pi\hbar$) and consists of a cylindrical core, which is the region of the normal phase of dimension ξ, and a superconducting region of dimension λ around the core, in which the superconducting current flows, screening the magnetic field (Fig. 2). The flux quantum Φ_0 is sometimes called the fluxoid. Quantization of the magnetic flux leads to a simple relation between the magnetic induction B and the average two-dimensional density of vortices, ρ_v in the mixed state

$$B = \Phi_0 \rho_v. \tag{1.7}$$

Here we can distinguish two cases. The London limit, $H_{ext} \ll H_{c2}$, where the average distance between vortices is

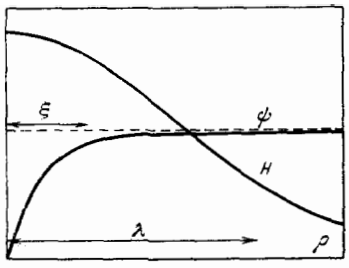

FIG. 2. Magnetic field $h(\rho)$ and the order parameter $|\psi|$ near the axis of the vortex filament.

large, $l \gg \xi$. Equation (1.3) is applicable everywhere except in the core of the vortex. The second is the Abrikosov limit $H_{ext} \lesssim H_{c2}$ the cores of the vortices overlap. In this case it is necessary to take into account the spatial variation of the order parameter ψ and analyze Eqs. (1.2).

As is well known, the Ginsburg–Landau theory is applicable for $1-(T/T_c) \ll 1$. This limitation on the temperature can be weakened if the true variations of $\lambda(T)$ and $\xi(T)$, and accordingly, $\alpha(T)$ and $\beta(T)$ are taken into account in Eqs. 1.2 and 1.3. In this case we find that the Ginsburg–Landau theory is in reasonably good quantitative agreement with experiment even at temperatures considerably below T_c ($T_c/2 < T < T_c$). The temperature range can be extended by introducing into the Ginsburg–Landau theory the three parameters $\varkappa_1(T)$, $\varkappa_2(T)$, and $\varkappa_3(T)$.[12] These parameters are related to the three macroscopic characteristics of a superconductor: H_{c2}, $(\partial M/\partial H)_{H_{c2}}$ and H_{c1}, respectively.

The solution of equations (1.2) in the limit $H_{ext} \lesssim H_{c2}$ and $\varkappa \gg 1$ was first derived by Abrikosov.[13] It was shown that $\mathbf{h}$ and $|\psi|^2$ are periodic two-dimensional functions in the plane perpendicular to $\mathbf{H}_{ext}$. The periodic solutions with the symmetry of an equilateral triangle (triangular lattice) or of a square are the energetically more favorable solutions. The triangular lattice has the absolute minimum in energy, but the energy difference is not much (of the order of 2%), and both structures have been observed experimentally. The solution has the form

$$h = B - \frac{1}{2\varkappa^2}(|\psi|^2 - \langle|\psi|^2\rangle), \tag{1.8}$$

where $|\psi|^2$ is determined by the double Fourier series

$$|\psi^{\square}|^2 = \langle|\psi|^2\rangle \sum_{n,m=-\infty}^{\infty} (-1)^{nm} \times \exp\left[-(n^2+m^2)\frac{\pi}{2}\right] \exp[2\pi i(\tilde{x}n + \tilde{y}m)], \tag{1.9a}$$

$$|\psi^{\triangle}|^2 = \langle|\psi|^2\rangle \sum_{n,m=-\infty}^{\infty} (-1)^{nm} \exp\left(-i\pi\frac{n}{2}\right) \times \exp\left[-(n^2+m^2-mn)\frac{\pi}{\sqrt{3}}\right] \exp[2\pi i(\tilde{X}n + \tilde{Y}m)] \tag{1.9b}$$

for the square and the triangular lattices, respectively, with the normalization

$$\langle|\psi|^2\rangle = b\frac{4\varkappa^2\pi}{1+\beta_g(2\varkappa^2-1)}, \tag{1.10}$$

where $\langle\ldots\rangle$ means an average over the spatial coordinate, β_g is a geometric factor, ($\beta_{\triangle} = 1.16$, $\beta_{\square} = 1.18$), and $b = (H_{c2} - B)/B$. For the case $H_{ext} \lesssim H_{c2}$, b is a small parameter. In formulas (1.9a) and (1.9b) the Cartesian coordinates x and y and the oblique coordinates $\tilde{Y}$ and $\tilde{X}$ are chosen so as to make the zeros of the function $|\psi|^2$ occur at integral points. The real dimensions of the unit cell of the lattice are determined from condition (1.7). The induction B and the external field H_{ext} are connected by the relation

$$H_{ext} = B + \frac{H_{c2} - B}{1+\beta_g(2\varkappa^2-1)}. \tag{1.11}$$

Expressions (1.8)–(1.11) are valid for $b \ll 1$, and they are the first terms in the expansion in powers of b (Ref. 14).

We shall solve the London equation (1.3) for the case where $H_{ext} \ll H_{c2}$ everywhere except in the cores of the vortices. The field in the vicinity of the core can be found by the use of Eqs. (1.2).[13] The vortex filament can be described by means of the London equation by the use of the boundary conditions on the surface of the core (the interface between the normal metal and the superconductor). In the limit $\xi \ll a$, this leads, as is well known, to a modification of Eq. (1.3)

$$\mathbf{h} + \lambda^2 \operatorname{curl}\operatorname{curl}\mathbf{h} = \Phi_0 \sum_i \delta(\boldsymbol{\rho} - \boldsymbol{\rho}_i); \tag{1.12}$$

where $\delta(\boldsymbol{\rho}-\boldsymbol{\rho}_i)$ is the two-dimension delta function corresponding to the ith vortex, $\boldsymbol{\rho}_i$ is its coordinate, and Φ_0 is directed along the axis of the vortex ($|\boldsymbol{\Phi}_0| = \Phi_0$). The solution $\mathbf{h}(\boldsymbol{\rho})$ of Eq. (1.12) has a logarithmic divergence at $\boldsymbol{\rho}_i$. The field inside the core is usually taken to be $h(\rho_{ix} + \xi, \rho_{iy})$. The solution of (1.12) for a rectangular vortex lattice is[4]

$$h = B\alpha^2 \sum_{n,m=-\infty}^{+\infty} \frac{\exp[2\pi i(\tilde{x}n + \tilde{y}m)]}{n^2 + m^2\tau^2 + \alpha^2}; \tag{1.13}$$

here a and b are the sides of the rectangular unit mesh, $\tau = a/b$, $\tilde{x} = x/a$, $\tilde{y} = y/b$, and $\alpha^2 = a^2/4\pi^2\lambda^2$. Equation (1.12) is linear, and therefore its solution can be written as a sum of solutions of Eq. (1.13) for two rectangular lattices arranged with the vertices of one on the intersections of the diagonals of the other. For $\tau = 1/\sqrt{3}$ we obtain the equilateral triangle lattice.

2. MUON METHOD FOR ISOTROPIC SUPERCONDUCTORS

Let us consider the characteristics of the muon spin rotation spectrum for a vortex lattice. The magnetic field in a periodic vortex lattice has three types of singular points: Maxima, located at the nodes of the vortex lattice; these correspond to the field in the core of the vortex; minima, in the centers of the squares or triangles forming the lattice and saddle points, in the middle of the edges of the unit cells. The distribution density of this function, that is, the corresponding Fourier spectrum of the polarization, has three Van Hove singularities (Fig. 3). The quantities ω_{min}, ω_{sad}, and ω_{max} are the fields (in units of the muon frequency) at the minimum point, the saddle point, and the maximum point, respectively.

Let us use formula (1.13) to find the characteristic frequencies of the Fourier spectra for the vortex lattice in the London limit. It is easy to carry out the summation over one of the indices:[15–17]

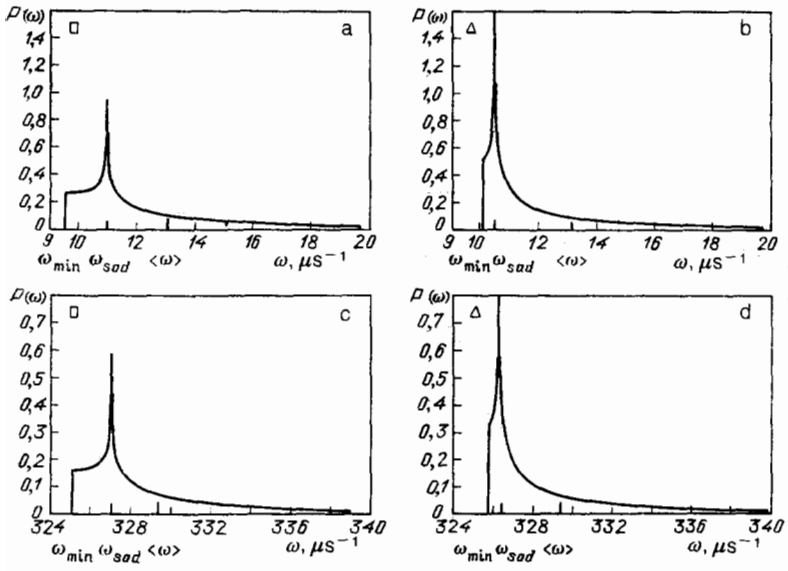

FIG. 3. Fourier spectra $P(\omega)$ for a square lattice (a, c), and a triangular lattice (b, d) in an isotropic superconductor; $\lambda = 1450$ Å, $\xi = 20$ Å, $H_{c1} = 335$ G. a,b) $H_{ext} = 400\ \mathrm{G} \gtrsim H_{c1}$. c,d) $H_{ext} = 4000\ \mathrm{G} \gg H_{c1}$. Formulas (2.3)–(2.4) were used.

$$\omega = \langle\omega\rangle + \langle\omega\rangle\left[\frac{\pi\alpha\,\mathrm{ch}\,[\alpha\pi\,(1-2\tilde{x})]}{\mathrm{sh}\,(\alpha\pi)} - 1 + 2\pi\alpha^2\sum_{m=1}^{\infty}\frac{\cos\,(2\pi m\tilde{y})\,\mathrm{ch}\,[\beta\pi\,(1-2\tilde{x})]}{\beta\,\mathrm{sh}\,(\beta\pi)}\right], \tag{2.1}$$

where $\beta^2 = \alpha^2 + m^2\tau^2$. Formula (2.1) greatly simplifies the calculation of $\omega(\rho)$. For fields that are far from H_{c1} $(\alpha^2 \ll 1)$ and the so-called intermediate field $H_{c1} \ll H_{ext} \ll H_{c2}$ one can carry out the summation over the second index and obtain an analytic expression for $\omega(\mathbf{p})$. For the two vortex lattice geometries the corresponding formulas are

$$\omega = \langle\omega\rangle + \gamma_\mu\frac{\Phi_0}{4\pi\lambda^2}\left[-\ln\frac{\vartheta_4\,(2\pi\tilde{y}\,|\,i)\,\vartheta_4\,(2\pi\tilde{x}\,|\,i) - \vartheta_2\,(2\pi\tilde{y}\,|\,i)\,\vartheta_2\,(2\pi\tilde{x}\,|\,i)}{\vartheta_4^2\,(0\,|\,i)}\right], \tag{2.2a}$$

$$\omega = \langle\omega\rangle + \gamma_\mu\frac{\Phi_0}{4\pi\lambda^2}\left[\frac{1}{3}\ln 2 - \ln\frac{\vartheta_4\,(2\pi\tilde{y}\,|\,i\tau)\,\vartheta_4\,(2\pi\tilde{x}\,|\,i/\tau) - \vartheta_2\,(2\pi\tilde{y}\,|\,i\tau)\,\vartheta_2\,(2\pi\tilde{x}\,|\,i/\tau)}{\tau^{1/2}\vartheta_2\,(0\,|\,i\tau)\,\vartheta_4\,(0\,|\,i\tau)}\right], \tag{2.2b}$$

where we have used the Jacobi ϑ function (see e.g., Ref. 18), and have set $\tau = 1/\sqrt{3}$.

Now, with the use of formulas (2.2) it is easy to find the characteristic frequencies of the Fourier spectrum:

$$\omega_{\min}^{\square} = \langle\omega\rangle - \gamma_\mu\frac{\Phi_0}{4\pi\lambda^2}\cdot\ln 2, \tag{2.3a}$$

$$\omega_{\min}^{\triangle} = \langle\omega\rangle - 0.79\,\gamma_\mu\frac{\Phi_0}{4\pi\lambda^2}\cdot\ln 2,$$

$$\omega_{\mathrm{sad}}^{\square} = \langle\omega\rangle - \frac{1}{2}\gamma_\mu\frac{\Phi_0}{4\pi\lambda^2}\cdot\ln 2, \tag{2.3b}$$

$$\omega_{\mathrm{sad}}^{\triangle} = \langle\omega\rangle - \frac{2}{3}\gamma_\mu\frac{\Phi_0}{4\pi\lambda^2}\cdot\ln 2,$$

$$\omega_{\max}^{\square} = \langle\omega\rangle + \gamma_\mu\frac{\Phi_0}{4\pi\lambda^2}\left(2\ln\frac{a}{2\sqrt{2}K\xi} + \frac{1}{3}\ln 2\right),$$

$$\omega_{\max}^{\triangle} = \langle\omega\rangle + \gamma_\mu\frac{\Phi_0}{4\pi\lambda^2}\cdot 2\ln\frac{\sqrt{3}a}{2\sqrt{2}K\xi}; \tag{2.3c}$$

where K is the complete elliptical integral in the parameters $\tau_\square = 1$ and $\tau_\triangle = 1/\sqrt{3}(k = \vartheta_2^2(0|i\tau)/\vartheta_3^2(0|i\tau)$, respectively).

Besides the frequencies, the experimenter may find interest in the Fourier amplitudes at $\omega_{\min}$ and $\omega_{\max}$:

$$P_{\min}^{\square} = \frac{4\pi\lambda^2}{\gamma_\mu\Phi_0}, \quad P_{\min}^{\triangle} = 2{,}44\,\frac{4\pi\lambda^2}{\gamma_\mu\Phi_0}, \tag{2.4a}$$

$$P_{\max}^{\square} = 2\,\frac{4\pi\lambda^2}{\gamma_\mu\Phi_0}\frac{\xi^2}{a^2}, \quad P_{\max}^{\triangle} = 2\,\frac{4\pi\lambda^2}{\gamma_\mu\Phi_0}\frac{\xi^2}{\sqrt{3}a^2}. \tag{2.4b}$$

It can be seen from Fig. 3 that it is possible to infer the lattice type from the shape of the spectrum. The spectrum for the triangular lattice differs from that of the square lattice by a much higher amplitude of $P_{\min}$ and a substantial shift of ω_{sad} towards $\omega_{\min}$. The corresponding curves of $P(t)$ are shown in Fig. 4. We note that the square lattice also differs by the presence of pronounced beats in $P(t)$. In the case of the triangular lattice the beats show up considerably later and are hard to see. After determining the type of lattice from formulas (2.3) and (2.4) one can calculate $\lambda(T)$ and $\xi(T)$.

The most useful formula from the experimental point of view is (2.3b), which connects ω_{sad} and $\langle\omega\rangle$. The actual experimental spectra, of course, are different from the ideal picture (see Fig. 3). The Van Hove singularities in the spectrum of $P(\omega)$ are smeared out because of unavoidable experimental errors and because the experiment does not yield $P(t)$ as a continuous function, but as a histogram, determined by the width of the time channel. Therefore, the points $\omega_{\max}$ and $\omega_{\min}$ can be determined with an accuracy equal to half the width of the broadening of the edges of the curve of $P(\omega)$. On the other hand, the maximum value of the density of $P(\omega)$ is determined very well even for the smeared-out peak. The carrier frequency $\langle\omega\rangle$ is experimentally determined with an accuracy to four places. Therefore, the value of $\langle\omega\rangle - \omega_{\mathrm{sad}}$ (see formula (2.3b)) is more convenient for the determination of λ.

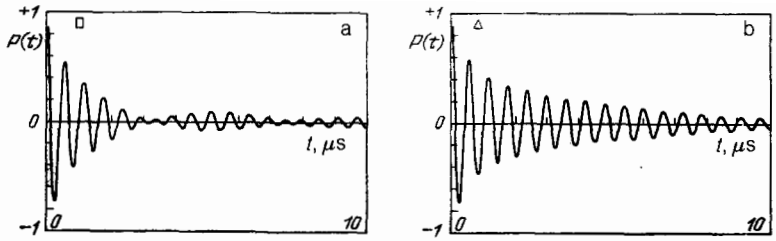

FIG. 4. Muon polarization $P(t)$ for a square lattice (a), and a triangular lattice (b); $\lambda = 1450$ Å, $\xi = 20$ Å, $H_{c1} = 335$ G, $H_{ext} = 400$ G.

For the case $\alpha^2 \ll 1$ the shape of $P(\omega)$ does not depend on the value of B. If B changes then the spectrum of $P(\omega)$ shifts in frequency as a whole, but the values of $\langle\omega\rangle - \omega_{sad}$, $\langle\omega\rangle - \omega_{min}$, and P_{min} remain unchanged. Thus, $P(t)$ is self-similar; it is the envelope of the oscillating function $P(t, H_{ext})$, which does not change when the carrier frequency is changed. (There is a distortion of $P(\omega)$ in the region of ω_{max}, but because of its small amplitude: $P_{max} \propto \xi^2/a^2$, the effect on the shape of $P(t)$ can be neglected at these frequencies).

We note that for $a \gg \xi$ the value of P_{max} (2.4b) is vanishingly small. Therefore, it is impossible in practice to determine ω_{max} or P_{max}, and hence ξ experimentally. To measure ξ one must operate in the range $H_{ext} \lesssim H_{c2}$, where $a \gtrsim \xi$.

Keeping the terms with $n, m = 0, \pm 1$ in (1.9) and using formula (1.8) we obtain

$$\omega^{\square}(\tilde{x}, \tilde{y}) = \langle\omega\rangle + (\omega_{ext} - \langle\omega\rangle)\,\delta_{\square}\,[\cos(2\pi\tilde{x}) + \cos(2\pi\tilde{y}) + \delta_{\square}\cos(2\pi\tilde{x})\cdot\cos(2\pi\tilde{y})], \quad (2.5a)$$

$$\omega^{\triangle}(\tilde{X}, \tilde{Y}) = \langle\omega\rangle + \{(\omega_{ext} - \langle\omega\rangle)\,\delta_{\triangle}\,[\cos(2\pi\tilde{X}) + \cos(2\pi\tilde{Y}) + \cos[2\pi(\tilde{X} + \tilde{Y})]\}, \quad (2.5b)$$

where $\delta_{\square} = 2\exp(-\pi/2)$, and $\delta_{\triangle} = 2\exp(-\pi/\sqrt{3})$.

The remaining terms in the series (1.9) can be neglected. It is easy to see that formulas (2.5) have an accuracy of $\approx 1\%$. Transforming in formula (I.3) to an integration over the isoline $\omega = \omega(\rho)$:

$$P(\omega) = \int \frac{dl}{|\operatorname{grad}\omega|} = \int \frac{dx}{|\partial\omega(\rho)/\partial y|}\,dx, \quad (2.6)$$

we obtain the Fourier spectrum corresponding to the fields (2.5) in the form

$$\tilde{P}^{\square}(\tilde{\omega}) = \frac{1}{\delta_{\square}\pi^2}(1+\tilde{\omega}^2)^{-1/2}\,K\left(\left\{\frac{1-[(\delta_{\square}^2-\tilde{\omega})^2/4\delta_{\square}^2]}{1+\tilde{\omega}}\right\}^{1/2}\right), \quad (2.7a)$$

$$\tilde{P}^{\triangle}(\tilde{\omega}) = \frac{2}{\delta_{\triangle}\pi^2}\,\frac{\delta_{\triangle}^{1/4}}{2R(\tilde{\omega})^{1/2}}\,K\left(\frac{1}{2}\left(\frac{T(\tilde{\omega})+2R(\tilde{\omega})}{R(\tilde{\omega})}\right)^{1/2}\right) \text{ for } \tilde{\omega} \geqslant \tilde{\omega}_{sad},$$
$$= \frac{2}{\delta_{\triangle}\pi^2}\,\frac{\delta_{\triangle}^{1/4}}{(T(\tilde{\omega})+2R(\tilde{\omega}))^{1/2}}\,K\left(2\left(\frac{R(\tilde{\omega})}{T(\tilde{\omega})+2R(\tilde{\omega})}\right)^{1/2}\right) \text{ for } \tilde{\omega} \leqslant \tilde{\omega}_{sad}; \quad (2.7b)$$

where $\tilde{\omega} = (\omega - \langle\omega\rangle)/(\omega_{ext} - \langle\omega\rangle)$,

$$R(\tilde{\omega}) = (2\tilde{\omega} + 3\delta_{\triangle})^{1/2}, \quad T(\tilde{\omega}) = \delta_{\triangle}^{1/2}\left(3 - \frac{\tilde{\omega}^2}{\delta_{\triangle}^2}\right),$$
$$\int \tilde{P}(\tilde{\omega})\,d\tilde{\omega} = 1,$$

and $K(\ldots)$ is the complete elliptical integral of the first kind. Below we present the characteristic frequencies and amplitudes of the spectra:

$$\begin{aligned}
&\tilde{\omega}_{min}^{\square} = \delta_{\square}^2 - 2\delta_{\square}, \quad \tilde{\omega}_{min}^{\triangle} = -\frac{3\delta_{\triangle}}{2},\\
&\tilde{\omega}_{sad}^{\square} = -\delta_{\square}^2, \quad \tilde{\omega}_{sad}^{\triangle} = -\delta_{\triangle},\\
&\tilde{\omega}_{max}^{\square} = 2\delta_{\square} + \delta_{\square}^2, \quad \tilde{\omega}_{max}^{\triangle} = 3\delta_{\triangle},\\
&\tilde{P}_{min}^{\square} = [2\pi\delta_{\square}(1-\delta_{\square})]^{-1}, \quad \tilde{P}_{min}^{\triangle} = 2(\sqrt{3}\pi\delta_{\triangle})^{-1},\\
&\tilde{P}_{max}^{\square} = [2\pi\delta_{\square}(1+\delta_{\square})]^{-1}, \quad \tilde{P}_{max}^{\triangle} = (2\sqrt{3}\pi\delta_{\triangle})^{-1}.
\end{aligned} \quad (2.8)$$

It can be seen that for $H_{ext} \lesssim H_{c2}$ we find that ω_{sad} still tends to shift towards ω_{min}, and P_{min} is still higher in the triangular lattice than in the square lattice.

From (2.5) one can easily obtain, using (I.2) an analytic expression for $P(t)$ (Ref. 19)

$$P^{\square}(t) = J_0^2(pt)\cos(\langle\omega\rangle t) + \delta_{\square}pt J_1^2(pt)\sin(\langle\omega\rangle t), \quad (2.9a)$$

$$P^{\triangle}(t) = J_0^3(pt)\cos(\langle\omega\rangle t) + pt J_1^2(pt)\sin(\langle\omega\rangle t), \quad (2.9b)$$

where $p = \delta_g(\omega_{ext} - \langle\omega\rangle)$. For the square lattice we have pronounced beats $\sim J_0^2(pt)$, while for the triangular lattice the beats are hardly visible, since the two terms in (2.9b) are comparable in magnitude.

After measurement of the carrier frequency $\langle\omega\rangle$ of the oscillations of the polarization, the Ginsburg–Landau parameter $\varkappa$ can be calculated from the formula (see (1.11))

$$\omega_{ext} - \langle\omega\rangle = \frac{\omega_{c2} - \langle\omega\rangle}{1 + \beta_g(2\varkappa^2 - 1)}. \quad (2.10)$$

Recalling that we obtained the penetration depth λ experimentally in intermediate fields, we see that we can use formula (2.10) to determine ξ of the superconductor. The difference $\omega_{ext} - \langle\omega\rangle$ determines the shape of the Fourier spectrum $P(\omega)$ and of the polarization $P(t)$, (2.7)–(2.9). By a comparison of the experimental and theoretical curves it is possible to judge whether the Ginsburg–Landau theory and the Abrikosov approximation are applicable.

3. THE MUON METHOD FOR ANISOTROPIC HIGH-T_c SUPERCONDUCTORS

Since the discovery of a new type of superconducting materials, the high-T_c superconductors, a large number of experimental papers have appeared, dealing with the muon method of studying these materials. However, what the values are for λ and ξ in these materials is still essentially an open question. The difficulties arise because, first, the high-T_c superconductors are highly anisotropic, and second, the experiments are almost always (with rare exceptions) carried out on polycrystalline samples consisting of a large number of randomly oriented single crystallites (granules).

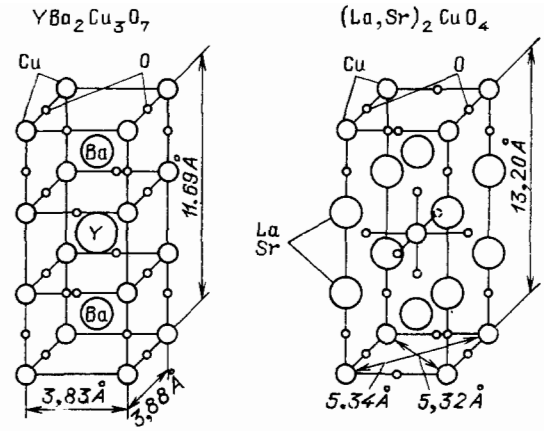

FIG. 5. Structure of the crystal lattices of $YBa_2Cu_3O_7$ and $(La,Sr)_2CuO_4$.

The anisotropy of a superconductor can be taken into account in the Ginsburg–Landau theory with the use of the effective mass tensor $m_{\gamma\delta}$. All the known high-T_c superconductors are, with high precision, uniaxially anisotropic superconductors. The principal values of the tensor $m_{\gamma\delta}$ are

$$m_a \approx m_b = m_{ab}, \quad m_c = (1+\chi)\, m_{ab}; \tag{3.1}$$

Here χ is the anisotropy parameter. In the ab plane and along the c axis we have for the critical fields and for $\lambda(T)$ and $\xi(T)$

$$\frac{H_{c1}^{c}}{H_{c1}^{ab}} \approx \frac{H_{c2}^{ab}}{H_{c2}^{c}} = \frac{\xi_{ab}}{\xi_c} = \frac{\lambda_c}{\lambda_{ab}} = \left(\frac{m_c}{m_{ab}}\right)^{1/2} = (1+\chi)^{1/2}. \tag{3.2}$$

For typical high-T_c superconductors the following estimates are usually used: for $YBa_2Cu_3O_7$, $\chi \approx 25$, and for $(La,Sr)_2CuO_4$, $\chi \approx 10$ (see Table I).

The free energy for an anisotropic superconductor is[20]

$$F = \int dV \Big[\alpha(T)(T-T_c)|\psi|^2 + \frac{\beta(T)}{2}|\psi|^4 + \frac{1}{4} m_{\gamma\delta}^{-1}\Big(i\hbar\nabla_\gamma - \frac{2e}{c}A_\gamma\Big)\psi^*\Big(-i\hbar\nabla_\delta - \frac{2e}{c}A_\delta\Big)\psi + \frac{h^2}{8\pi}\Big]. \tag{3.3}$$

Standard variational procedure gives the Ginsburg–Landau equations

$$\alpha(T)(T-T_c)\psi + \beta(T)|\psi|^2 + \frac{1}{4} m_{\gamma\delta}^{-1}\Big(-i\hbar\nabla_\delta - \frac{2e}{c}A_\delta\Big)\Big(-i\hbar\nabla_\gamma - \frac{2e}{c}A_\gamma\Big)\psi = 0, \tag{3.4a}$$

$$\frac{\mathrm{curl}_\gamma \mathbf{h}}{4\pi} = \frac{j_\gamma}{c} = \frac{e\hbar}{2ic} m_{\gamma\delta}^{-1}(\psi^*\nabla_\delta\psi - \psi\nabla_\delta\psi^*) - \frac{2e^2}{c^2} m_{\gamma\delta}^{-1} A_\delta |\psi|^2. \tag{3.4b}$$

By analogy with the isotropic case we introduce the tensors

$$\xi_{\gamma\delta}^2 = \frac{\hbar^2 m_{\gamma\delta}^{-1}}{4\alpha(T)(T_c - T)}, \quad \lambda_{\gamma\delta}^2 = \frac{c^2 m_{\gamma\delta}}{8\pi e^2 |\psi_0|^2}, \quad |\psi_0|^2 = \frac{\alpha(T)(T_c - T)}{\beta(T)}. \tag{3.5}$$

The principal values of the tensors $\xi_{\gamma\delta}^2$ and $\lambda_{\gamma\delta}^2$, are the squares of the penetration depth and the correlation lengths in the ab plane and along the axis of anisotropy (see (3.2)). The corresponding modified London equation for an anisotropic superconductor has the form[21]

$$\mathbf{h} + \mathrm{curl}\,\hat{\lambda}^2 \cdot \mathrm{curl}\,\mathbf{h} = \Phi_0 \sum \delta(\rho - \rho_i), \tag{3.6}$$

where $\hat{\lambda}^2$ is the tensor operator with components $\lambda_{\gamma\delta}^2$. We note that the direction of the induction vector **B** and the axes of the vortex filaments of the high-T_c superconductor in the general case are not the same as the direction of the external magnetic field $\mathbf{H}_{ext}$. Moreover, the macroscopic field **h** in the vortex lattice has components that are perpendicular to **B**. Therefore, $\langle\omega\rangle$ differs from $\gamma_\mu \mathbf{B}$, that is, it is not equal to the precession frequency in the field **B**, here ($\langle\omega\rangle = \gamma_\mu\langle\mathbf{h}\rangle$). Exceptions are the cases with the orientations $\mathbf{H}_{ext} \| \mathbf{c}$ and $\mathbf{H}_{ext} \perp \mathbf{c}$ (the external field is parallel to the axis of anisotropy or the ab plane).

Let us choose a Cartesian coordinate system x,y,z such that $c_y = 0$ (Fig. 6); that is, **c** and $\mathbf{H}_{ext}$ lie in the xz plane and the induction **B** is directed along the z axis and is perpendicular to the plane xy of the vortex lattice.

TABLE I.

Reference	Sample	λ_{eff}, A	λ_{ab}, A	λ_c, Å	T, K
	$YBa_2Cu_3O_7$:				
[55]	Polycrystalline			⩾6000	0
[58]	»		908		14,8
[54]	»		700		10
[53]	»	1400	1065		6
[47]	»	1200			0
[45]	»	1550	1300	5000—8000	0
[24]	Single Crystal		1430	⩾7000	0
	$La_{1,85}Sr_{0,15}CuO_4$:				
[56]	Polycrystalline	3100			0
[54]	»		1300		0
[49]	»	2500			6
[50]	»	2000			10
[55]	»			⩾3500	0
[51]	»	2650			0
[52]	»	2300			13
[58]	»		3690		5

The solution of Eq. (3.6) for a rectangular vortex lattice is[22]

$$h_x(\rho) = \Phi_0 c_z c_x S_2(\rho) S^{-1},$$
$$h_y(\rho) = -\Phi_0 c_z c_x S_3(\rho) S^{-1}, \qquad (3.7)$$
$$h_z(\rho) = \Phi_0 (S_1(\rho) - c_x^2 S_2(\rho)) S^{-1},$$

where we have introduced the notation

$$S_1 = \alpha^2 \sum_{n,m} \frac{\exp[2\pi i (n\tilde{x} + m\tilde{y})]}{n^2 + \beta^2},$$
$$S_2 = \frac{\chi}{\chi_2} \alpha^2 \tau^2 \sum_{n,m} \frac{m^2 \exp[2\pi i (n\tilde{x} + m\tilde{y})]}{(n^2 + \beta^2)(n^2 + \beta'^2)},$$
$$S_3 = \frac{\chi}{\chi_2} \alpha^2 \tau \sum_{n,m} \frac{nm [\exp 2\pi i (n\tilde{x} + m\tilde{y})]}{(n^2 + \beta^2)(n^2 + \beta'^2)},$$

$\tilde{x} = x/a$, $\tilde{y} = y/b$, $\alpha^2 = a^2/4\pi^2\lambda_{ab}^2$, $\tau = a/b$, $\chi_1 = 1 + \chi$, $\chi_2 = 1 + c_z^2\chi$, $\beta^2 = \alpha^2 + m^2\tau^2$, $\beta'^2 = (\alpha^2 + \chi_1 m^2 \tau^2)/\chi_2$, and the summation is taken over all integral n and m.

The vortex lattice of an anisotropic uniaxial superconductor is obtained from an equilateral triangular or a square lattice that is stretched along the y axis by a factor $[(1+\chi)/(1+c_z^2\chi)]^{1/2}$ and has the symmetry of a rectangle or an isosceles triangle. The minimum in energy corresponds to the orientation of the original regular lattice with the x axis parallel to the edge of the unit cell.[23] The geometric size of the unit cell, as before, is given by relation (1.7).

For an arbitrary orientation of the crystal the fields can be calculated by formulas (3.7) only numerically (suitable formulas for the numerical calculations are given in Ref. 22). We note only the qualitative features that arise as a result of the anisotropy. The function $\omega(\rho)$ now has two nonequivalent saddle points, and so there are two Van Hove divergences in the Fourier spectrum $P(\omega)$ (Fig. 7). In the case of intermediate fields ($\alpha^2 \ll 1$) the relative positions of the characteristic frequencies of the spectrum $\langle\omega\rangle$, $\omega_{\min}$, ω_{sad1}, and ω_{sad2} do not depend on the applied field, just as in an isotropic superconductor. Therefore the function $P(t)$ is self-similar. It must be emphasized that the time dependence of the polarization, $P(t)$ of an anisotropic superconductor

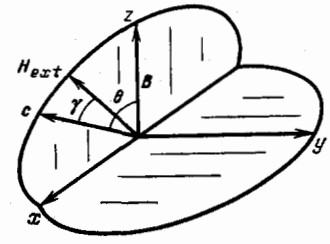

FIG. 6. Orientation of the (x,y) plane, of the vortex lattice and the magnetic induction $\mathbf{B}$ relative to $\mathbf{H}_{\text{ext}}$ and the axis of anisotropy, $\mathbf{c}$.

looks qualitatively like that for an isotropic semiconductor, and therefore it is easy to obtain information directly from the Fourier spectrum.

If we apply the external-field approximation to the limiting orientations $\mathbf{H}_{\text{ext}} \| \mathbf{c}$ and $\mathbf{H}_{\text{ext}} \perp \mathbf{c}$, the Van Hove divergences of the function $\mathbf{P}(\omega)$ merge together and we have the Fourier spectrum of an isotropic superconductor. In fact, the case $\mathbf{H}_{\text{ext}} \| \mathbf{c}$ is equivalent to the isotropic case. Substituting $c_z = 1$ and $c_x = 0$ in formulas (3.7) we obtain expression (1.3) with the replacement $\lambda \to \lambda_{ab}$. In addition, the case $\mathbf{H}_{\text{ext}} \perp \mathbf{c}$ reduces to the isotropic case by the transformation of coordinates

$$\tilde{x} \to \tilde{x}, \quad \tilde{y} \to \tilde{y}(1+\chi)^{1/2}. \qquad (3.8)$$

Substituting $c_z = 0$ and $c_x = 1$ into formulas (3.7) we have

$$h_x = h_y = 0,$$
$$h_z = \frac{\Phi_0}{S}(S_1(\rho) - S_2(\rho)) = \frac{\Phi_0}{S}\alpha^2 \sum_{n,m} \frac{\exp[2\pi i (n\tilde{x} + m\tilde{y})]}{n^2 + m^2\tau'^2 + \alpha^2}, \qquad (3.9)$$

where $\tau'^2 = (1+\chi)a^2/b^2$ in accordance with the transformation (3.8). Thus, for the characteristic frequencies and the amplitudes of the Fourier spectrum of an anisotropic uniaxial superconductor we have the following expressions

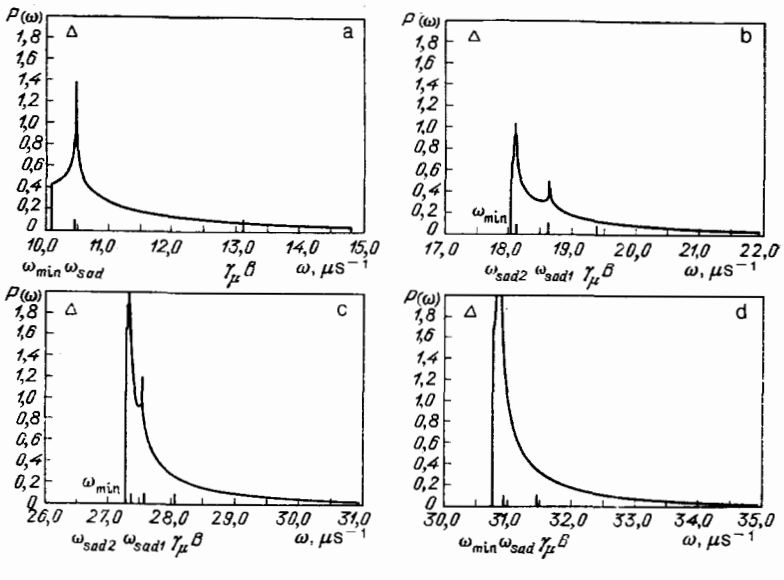

FIG. 7. Fourier spectra $P(\omega)$ for an anisotropic superconductor; $\lambda = 1450$ Å, $\xi = 20$ Å, $\lambda_c/\lambda_{ab} = (1+\chi)^{1/2} = 5$, $H_{c1} = 335$ G, $H_{\text{ext}} = 400$ G, for various angles $\gamma = f > a$: a) $\gamma = 0$; b) $\gamma = 30°$; c) $\gamma = 60°$; d) $\gamma = 90°$.

$$\omega_{\min}^{\square} = \langle\omega\rangle - \nu\gamma_\mu \frac{\Phi_0}{4\pi\lambda_{ab}^2} \cdot \ln 2,$$

$$\omega_{\min}^{\triangle} = \langle\omega\rangle - 0{,}79\nu\gamma_\mu \frac{\Phi_0}{4\pi\lambda_{ab}^2} \cdot \ln 2,$$

$$\omega_{\text{sad}}^{\square} = \langle\omega\rangle - \frac{1}{2}\nu\gamma_\mu \frac{\Phi_0}{4\pi\lambda_{ab}^2} \cdot \ln 2, \tag{3.10}$$

$$\omega_{\text{sad}}^{\triangle} = \langle\omega\rangle - \frac{2}{3}\nu\gamma_\mu \frac{\Phi_0}{4\pi\lambda_{ab}^2} \cdot \ln 2,$$

$$P_{\min}^{\square} = \frac{4\pi\lambda_{ab}^2}{\nu\gamma_\mu\Phi_0},$$

$$P_{\min}^{\triangle} = 2{,}44\,\frac{4\pi\lambda_{ab}^2}{\nu\gamma_\mu\Phi_0},$$

$$\nu = 1, \qquad \frac{\nu}{\lambda_{ab}^2} = \frac{1}{\lambda_{ab}^2} \quad \text{for } \mathbf{H}_{\text{ext}} \parallel \mathbf{c},$$

$$= (1+\chi)^{-1/2}, \qquad = \frac{1}{\lambda_{ab}\lambda_c} \quad \text{for } \mathbf{H}_{\text{ex}} \perp \mathbf{c}.$$

where $\nu = 1$ and $\nu/\lambda_{ab}^2 = 1/\lambda_{ab}^2$ for $\mathbf{H}_{\text{ext}} \parallel \mathbf{c}$, and $\nu = (1+\chi)^{1/2}$ and $\nu/\lambda_{ab}^2 = 1/\lambda_{ab}\lambda_c$ for $\mathbf{H}_{\text{ex}} \perp \mathbf{c}$.

For fields $H_{\text{ext}} \lesssim H_{c2}$ the solution of the Ginsburg–Landau equations (3.4) in the cases of $\mathbf{H}_{\text{ext}} \parallel \mathbf{c}$ and $\mathbf{H}_{\text{ext}} \perp \mathbf{c}$ also have a simple form:

$$h = B - \frac{1}{2\tilde{\varkappa}^2}(|\psi|^2 - \langle|\psi|^2\rangle), \tag{3.11}$$

$$\langle|\psi|^2\rangle = \frac{4\tilde{\varkappa}^2\pi}{1+\beta_g(2\tilde{\varkappa}^2-1)}, \tag{3.12}$$

$$H_{\text{ext}} = B + \frac{\tilde{H}_{c2} - B}{1+\beta_g(2\tilde{\varkappa}^2-1)}, \tag{3.13}$$

where $\tilde{\varkappa} = \lambda_{ab}/\xi_{ab}$, and $\tilde{H}_{c2} = \Phi_0/2\pi\xi_{ab}^2$ for $\mathbf{H}_{\text{ext}} \parallel \mathbf{c}$, and $\tilde{\varkappa} = \lambda_{ab}/\xi_c$, and $\tilde{H}_{c2} = \Phi_0/2\pi\xi_{ab}\xi_c$ for $\mathbf{H}_{\text{ext}} \perp \mathbf{c}$, and $|\psi|^2$ is defined by formulas (1.9). The change in scale along the y axis in the case $\mathbf{H}_{\text{ext}} \perp \mathbf{c}$ (see (3.8)) is carried out according to a rule that is formulated for fields $H_{\text{ext}} \ll H_{c2}$. The Fourier spectrum $P(\omega)$ and the polarization $P(t)$ are described by formulas (2.7)–(2.9) for an isotropic superconductor.

From this discussion it is clear that the most complete information can be obtained by using single crystal samples. However, to the present time almost all μ SR experiments (except that reported in Ref. 24) have used polycrystalline samples. We shall, therefore, consider what information can be obtained with the use of polycrystalline samples. A quantitative analysis is difficult because of the lack of reliable theoretical models for the behavior of a magnetic field in the interior of the sample. On the boundaries of the single crystals forming the polycrystalline sample the magnetic field can differ from H_{ext} both in magnitude and direction, and thus it is in general not entirely clear how to carry out the averaging. Moreover, the influence of the demagnetizing factor of the microparticles introduces an additional uncertainty in the pattern of the distribution of the microscopic field $\mathbf{h}(\mathbf{r})$. We shall, therefore, make only some qualitative remarks.

The lower critical field of an anisotropic superconductor depends on the angle between $\mathbf{H}_{\text{ext}}$ and $\mathbf{c}$: $\gamma(H_{c1}^{ab} \leqslant H_{c1}(\gamma) \leqslant H_{c1}^{c})$, and for $H_{c1}^{ab} \leqslant H_{\text{ext}} \leqslant H_{c1}$ the magnetic field penetrates only into some of the microparticles, while the Meissner phase remains in the rest. Experimentally this situation will show up as a growth of the amplitude $P(t)$ of the precessing component from zero at $H_{\text{ext}} = H_{c1}^{b}$ and as a saturation at $H_{\text{ext}} = H_{c1}^{c}$. Thus, from the amplitude saturation curve one can infer the characteristics of the superconductor. Following Ref. 21 we write $H_{c1}(\gamma)$ in the form

$$H_{c1}(\gamma) = H_{c1}^{c}(1+\chi\sin^2\gamma)^{-1/2},$$

$$H_{c1}^{c} = \frac{\Phi_0}{4\pi\lambda_{ab}^2}\ln\varkappa, \quad H_{c1}^{ab} = \frac{\Phi_0}{4\pi\lambda_c\lambda_{ab}}\ln\varkappa. \tag{3.14}$$

Making the crude assumption that all the microparticles are in the same field H_{ext}, and neglecting the demagnetizing factor, we have an expression for the fraction of the particles into which the field penetrates[22]

$$n = \left(\frac{1+\chi}{\chi}\right)^{1/2}\left[1 - \left(\frac{H_{c1}^{ab}}{H_{\text{ext}}}\right)^2\right]^{1/2} \quad \text{for } H_{c1}^{ab} \leqslant H_{\text{ext}} \leqslant H_{c1}^{c}. \tag{3.15}$$

Here $n = 0$ for $H_{\text{ext}} \leqslant H_{c1}^{ab}$ and $n = 1$ for $H_{\text{ext}} \geqslant H_{c1}^{c}$. It is clear that the relative amplitude $A(H_{\text{ext}})$ of the precessing component increases with the same slope as n, but, because of the change in the direction of $\mathbf{h}(\mathbf{n})$ within the single crystallites, n does not determine the field uniquely. One can only state (neglecting the demagnetizing factor) that in the initial increase in $A(H_{\text{ext}})$ corresponds to the field $H_{\text{ext}} \approx H_{c1}^{ab}$ and saturation to $H_{\text{ext}} \approx H_{c1}^{c}$.

Under the same assumptions, the Fourier spectrum of a polycrystalline sample can be obtained by averaging $P(\omega)$ for a single crystal over the various angles γ. Taking into account that the relative weighting of microparticles with orientation γ is proportional to $\sin\gamma$, we have a smooth increase in the Fourier component from zero for $\omega = \omega_{\min}^{c}(H_{\text{ext}})$ and a peak value that is shifted towards $\omega_{\text{sad}}^{ab}(H_{\text{ext}})$.

4. PINNING AND DISTORTION OF THE VORTEX STRUCTURES

A large number of papers have treated the topic of pinning in type II superconductors. Here two main questions arise. First is the theoretical determination of the parameters of the distorted lattice on the basis of the theory of collective pinning[25] for given pinning parameters in the sample. In this model the vortices are regarded as essentially rigid and parallel to each other, and the pinning is weak. The elastic properties are characterized by an elasticity matrix $\Phi_{\alpha\beta}(\mathbf{k})$ (here $\mathbf{k}$ is the wave vector, and $\alpha, \beta = x,y,z$). The distortion of the lattice is characterized by a correlation function of the displacement field. A detailed analysis of this problem can be found in Refs. 26–29. Expressions have been derived for the elasticity matrix and the correlation function. Analogous expressions near H_{c2} for $T \leqslant 0.625\ T_c$ in the BCS approximation were derived in Ref. 30. The smearing of the muon spectrum for small distortions of the regular lattice depends on the local magnetic field h. The expression for the second moment $\sigma(h)$ of the smearing was obtained in Ref. 31. The problem of temperature-induced fluctuations of the lattice and muon diffusion has been discussed in Refs. 31–35. It was shown that the frequency of the fluctuations of the lattice, particularly in high-T_c superconductors, is much higher than the frequency of the muon precession, and therefore

these fluctuations have no influence on the spin of the muon. The second problem that arises is to estimate the value of the critical current density $\mathbf{j}_c$ and determine its dependence on the external magnetic field within the theory of collective pinning.[29,36]

It has been shown experimentally[36,37] that for a certain field B_{c0} a sharp jump is observed in the critical current, and this jump is usually attributed to a transition from two-dimensional to three-dimensional pinning. No consistent theory of three-dimensional pinning has yet been put forth. Computer simulations have been carried out, however, and their results are in qualitative agreement with experimental data, and they support the hypothesized cause of the jump in $\mathbf{j}_c$.[38]

The muon method is extremely convenient for investigations of the structure of vortex lattices in the presence of pinning. Let us consider an idealized model of a two-dimensional vortex lattice with randomly arranged (uncorrelated) vortices. Of course, this model has a limited range of applicability, primarily because the bending of the vortices is ignored ("three-dimensional" pinning). However, for thin plates ($\mathbf{H}_{ext} \| \mathbf{z}$ and perpendicular to the plane of the plate) the two-dimensional structure is preserved if the thickness d of the sample satisfies the condition $d/2 < L_c$, where L_c is the longitudinal correlation length of pinning (not related to the correlation length ξ in the Ginsburg–Landau theory).[29] The assumption of an uncorrelated vortex structure presupposes that the "excluded volume," where the vortices strongly repel each other, is small. This assumption is almost always valid in weak and intermediate fields, as long as the density ρ of the vortices is not substantially greater than λ^{-2}. A quantitative estimate will be given later. The model we are considering is helpful for estimating the different kinds of arrangements of the local fields for the case of strong pinning in real samples. We shall consider the case of external fields $H_{ext} < 0.25 H_{c2}$, where the London equation is applicable over essentially the entire volume of the sample.[28] It is obvious that $\langle h \rangle = H_{ext}$ even for $H_{ext} < H_{c1}$. Neglecting edge effects, we can assume that the vortex structure is uniform over the volume of the plate. The analysis that follows is valid for isotropic as well as anisotropic superconductors if the external field is directed along one of the principal axes.[22] The latter case is of particular interest in the study of high-T_c superconductors. We also note that for high-T_c, superconductors, where H_{c2} is very high, the London approximation is valid for a broad range of H_{ext}.

The local magnetic field in the London limit is a superposition of the fields from the separate vortices

$$h(\rho) = \sum_i h_s(|\rho - \rho_i|). \tag{4.1}$$

The field of an individual vortex is

$$h_s(\rho) = \frac{\Phi_0}{2\pi\lambda^2} K_0\left(\frac{\rho}{\lambda}\right), \tag{4.2}$$

where K_0 is the modified Bessel function.

To find the probability density for the distribution of the internal field $W(h)$ for a stochastic lattice of uncorrelated vortices we shall use the method of Holtzmark.[39] For the function $W(h)$ we have the well-known relation

$$W(h) = \int\int \dots \int\int \delta\left(h - \sum_{i=1}^{N} h_i\right) W_i(h_i)\, dh_1\, dh_2 \dots dh_N. \tag{4.3}$$

For the Fourier transform we have

$$\widetilde{W}(\nu_h) = \frac{1}{2\pi} \int W(h) e^{i\nu_h h}\, dh \tag{4.4}$$

and obtain the convenient formula

$$\widetilde{W}(\nu_h) = \prod_{i=1}^{N} \widetilde{W}_i(\nu_h), \tag{4.5}$$

where

$$\widetilde{W}_i(\nu_h) = \frac{1}{2\pi} \int W_i(h) e^{i\nu_h h}\, dh. \tag{4.6}$$

Let us choose a region of sufficiently large radius R_N. The number of vortices within the region is $N = \pi\rho_v R_N^2$, where $\rho_v = H_{ext}/\Phi_0$ is the density of vortices.

One can readily derive the distribution function for the field $\widetilde{W}_i(\nu_h)$:

$$\widetilde{W}_i(\nu_h) = \frac{2}{R_N^2} \int_0^{R_N} \int_0^{2\pi} e^{i\nu_h h_s(\rho)} \rho\, d\rho \frac{d\varphi}{2\pi}. \tag{4.7}$$

Taking into account that the integrand is independent of φ and taking the upper limit of integration over ρ to be ∞ we have

$$\widetilde{W}_i(\nu_h) = 1 - \frac{2}{R_N^2} \int_0^{\infty} (1 - e^{i\nu_h h_s(\rho)}) \rho\, d\rho. \tag{4.8}$$

Substituting (4.8) into (4.5) and going to the limit $N \to \infty$ we have

$$\widetilde{W}(\nu_h) = \exp\left[-2\pi\rho_v \int_0^{\infty} (1 - e^{i\nu_h h_s(r)}) r\, dr\right]. \tag{4.9}$$

The distribution of the internal fields is obtained by the inverse Fourier transformation

$$W(h) = \int \widetilde{W}(\nu_h) e^{-ih\nu_h}\, d\nu_h. \tag{4.10}$$

In the present case the integrals in (4.9) and (4.10) cannot be expressed in terms of elementary or known special functions. The results of numerical calculations for specific values of the parameters λ, ξ, and H_{ext} are shown in Fig. 8. However, the second moment $\langle \Delta h^2 \rangle$ can be derived analytically. For this purpose we take the average $h^2(\rho)$ over the sample. From formulas (4.1) and (4.2) we have

$$h^2(\rho) = \sum_i h_s^2(|\rho - \rho_i|) + \sum_j \sum_{i \neq j} h_s(|\rho - \rho_i|) h_s(|\rho - \rho_j|). \tag{4.11}$$

Averaging the first term in (4.11) gives

$$\left\langle \sum_i h_s^2(|\rho - \rho_i|) \right\rangle = \pi\rho_v\lambda^2. \tag{4.12}$$

The second term in (4.11), as expected, is proportional to ρ_v^2, and, precisely, is equal to $\langle h \rangle^2$ (this result can be obtained by direct calculation). In the end we obtain the simple and beautiful result for $\langle \Delta h^2 \rangle$:

$$\langle \Delta h^2 \rangle = \frac{\Phi_0^2 \rho_v}{4\pi\lambda^2},$$

or

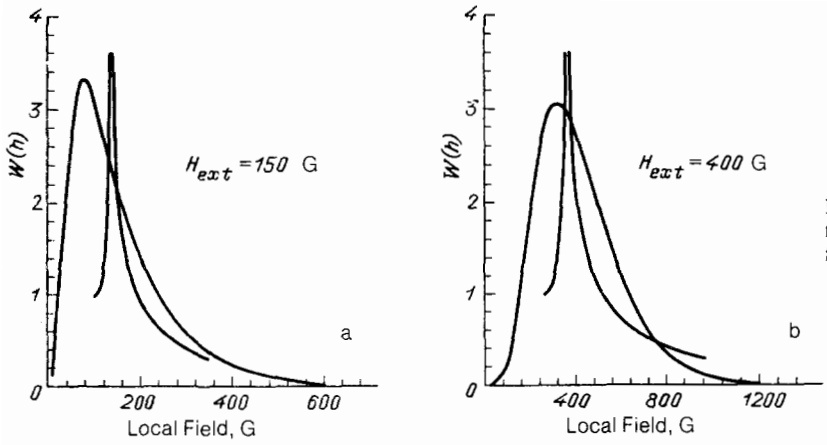

FIG. 8. Distribution function $W(h)$ of the local magnetic field in a superconducting sample ($\lambda = 1450$ Å, $\xi = 20$ Å) for a triangular and a random lattice.

$$\langle \Delta h^2 \rangle = \frac{H_{\rm ext} H_c}{\ln \varkappa} . \tag{4.13}$$

A comparison of the distribution function $W(h)$ with the distribution functions for the triangular and square lattices[11,15,29] reveals significant differences: first, the logarithmic Van Hove singularities are replaced by smooth maxima, and, naturally, the jumps in the distribution function, corresponding to the maximum and minimum of the local field, disappear. Second, for a random lattice an important factor in the analysis of the experiment is the difference between the average field and the most probable field $\langle h \rangle - \mathfrak{h}$ (here $W(\mathfrak{h}) = W_{\max}$) can turn out to be 2–10 times larger than in the case of a regular lattice. Third, $\langle \Delta h^2 \rangle_{\rm rand} \gg \langle \Delta h^2 \rangle_{\rm reg}$, and finally the character of the dependence $\langle \Delta h^2 \rangle$ on the external magnetic field is different from that for regular lattices. In Ref. 23 we find the incorrect statement that for a random lattice $\langle \Delta h^2 \rangle$ does not depend on the external field.

Let us now return to the question of the applicability of the model of a lattice of uncorrelated vortices. A good criterion is the free energy, but for all other parameters being equal ($H_{\rm ext}$, λ, ξ, etc.), it can be entirely replaced with the energy of interaction of the vortices. For the interaction energy we use the expression in Ref. 40. For the volume density of the interaction energy we have

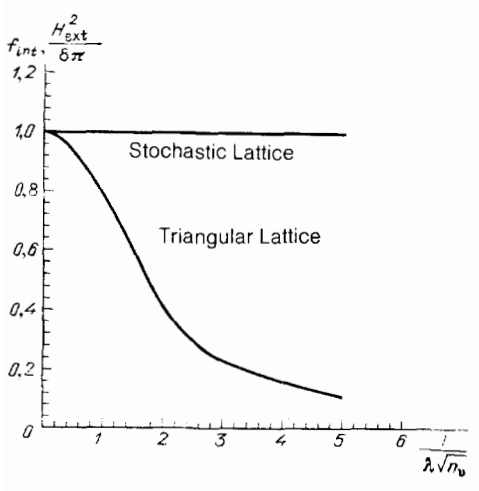

FIG. 9. Volume density of the interaction energy of vortices as a function of the external magnetic field in units of $H_{\rm ext}^2/8\pi$ in the approximation $\xi \ll \lambda$.

$$f_{\rm int} = \rho_v \frac{d\Phi_0^2}{16\pi^2\lambda^2} \sum_i K_0\left(\frac{\rho_i}{\lambda}\right) . \tag{4.14}$$

For the density of the interaction energy in a random lattice an averaging leads to a replacement of the summation by an integral. We have as a result

$$f_{\rm int} = \frac{1}{8\pi} \mathbf{H}_{\rm ext}^2 . \tag{4.15}$$

It was not possible to calculate the interaction energy analytically for an ordered lattice. The results of a computer calculation are shown in Fig. 9. For an external field of the order of H_{c1} the difference between the ordered and the random lattices is about 20%. The pinning must compensate just this amount. Therefore, if the pinning parameters are known it is not a difficult matter to determine whether it is possible to form a random vortex structure.

To verify these calculations we carried out a computer modeling of the fields in a random lattice. As shown in Fig. 10, we obtained agreement with a high degree of accuracy.

The results obtained show that the spectra and, consequently, the time dependence of the muon polarization $\mathbf{P}(t)$ in uncorrelated vortex lattices is quite different from the behavior of $\mathbf{P}(t)$ in regular structures. As can be seen, with the muon method one can observe strong pinning and investigate its characteristics.

Numerical calculations have shown that for these lattices the spectrum of $W(h)$ is close to a Gaussian distribution, and therefore it is correct to approximate the polarization by the function $e^{-\sigma^2 t^2}$, which is frequently used in analyzing the experimental data.

We shall now examine the possibilities of the μ SR method for the determination of the rate and the characteristics of creep of the vortex lattice during the conduction of current. As is well known, the onset of resistance and the value of the critical current for real superconductors is associated with the vortex creep[41] resulting from action of the Lorentz force on the vortices. It is also obvious that in real samples there are pinning centers of various strengths, and the creep starts with the separation from the pinning centers of the most weakly bound vortices, although the latter can then become attached to stronger centers. As the current is further increased all the vortices of the lattice participate in the motion, and for $\mathbf{j} = \mathbf{j}_c$ the superconductivity is destroyed.

It is clear that the study of creep is of primary impor-

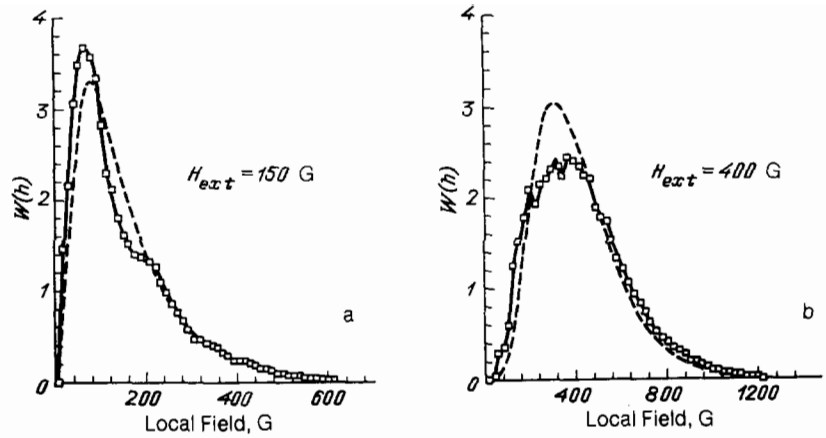

FIG. 10. Distribution function $W(h)$, obtained by Monte Carlo modeling of the internal fields for $\lambda = 1450$ Å, $\xi = 20$ Å, compared to the results obtained by the Holtzmark method.

tance for all the problems in the technical aspects of superconductivity. However, as far as we know, there is no method in existence by which one can study directly the creep of a vortex lattice. In particular, to determine the most important characteristic, the creep rate V_c, a phenomenological approach and empirical relations are used.

As we shall show, the μ SR method holds out the greatest promise for the study of the characteristics of creep. Below, we shall consider isotropic superconductors, but it should be noted that the results obtained can be carried over practically without modification to polycrystalline anisotropic high-T_c superconductors.

The appearance of resistance with creep is related to viscous losses (energy dissipation) in the motion of the vortices.[4] To estimate the viscosity we use the empirical formula[41]

$$\eta_c = \frac{\pi\hbar H_{c2}\sigma}{ec}, \tag{4.16}$$

where σ is the conductivity of the sample in the normal state.

The Lorentz force acting on a unit length of a vortex is

$$\mathbf{f}_L = \frac{\Phi_0}{c}[\mathbf{nj}], \tag{4.17}$$

where $\mathbf{n}$ is the unit vector directed along the core of the vortex and $\mathbf{j}$ is the current density. Thus, the velocity of a vortex is given by the formula

$$\mathbf{V}_c = \frac{\mathbf{f}_L}{\eta_c}. \tag{4.18}$$

Experiments have been carried out in which a variation in the muon depolarization rate has been observed during the passage of a current through the sample (see section 5c of Ref. 42), but there was no direct observation of the creep *per se*. It is obvious that in the presence of creep the magnetic field on a muon at rest is not stationary, and as a result the Fourier spectrum of the muon polarization changes. In what follows we shall assume that the muons do not diffuse. In a superconductor with a large concentration of defects this assumption is clearly satisfied at a sufficiently low temperature. A rough estimate of the characteristic time of variation of the field at the muon in the presence of creep yields the result

$$\tau_c \approx \frac{d}{V_c} \approx \frac{H_{c2}\sigma}{jH^{1/2}}\left(\frac{\pi\hbar}{ec}\right)^{1/2}, \tag{4.19}$$

where d is the characteristic dimension of the lattice, $d \approx (\Phi_0/H)^{1/2}$.

A numerical estimate gives $\tau_c \approx 10^{-7}$–10^{-8} s, both for type II superconductors ($H_{c2} \sim 10^4$ G, $\sigma \sim 10^5$ S/cm, $j \sim 10^3$ A/cm^2, and $H \sim 300$ G) and for high-T_c superconductors ($H_{c2} \sim 10^5$ G, $\sigma \sim 10^{-3}$ S/cm, $j \sim 10^2$ A/cm^2, and $H \sim 300$ G). The estimates thus arrived at agree in order of magnitude with the experimental data for the creep rate.[41] As can be seen, one can attain either a slow creep ($\tau_c \gg \tau_\mu$) or a fast creep ($\tau_c \ll \tau_\mu$) by varying j or H.

The most illustrative and interesting results are obtained for the case of fast creep. The field at the muon can conveniently be written as the sum of a constant component and a rapidly varying component

$$h(t) = \langle h\rangle + \delta h(t). \tag{4.20}$$

The characteristic time of variation of the field is $\sigma_c \ll \tau_\mu$, and the mean square value $\langle \delta h^2\rangle$, the second moment of the distribution of the field in the stationary lattice, does not exceed H_{c1}^2. For the polarization of the muon we have the well known formulas

$$P_+(t) = P_+(0)\exp\left(i\gamma_\mu \int_0^t h(\tau)\,d\tau\right), \tag{4.21}$$

$$P_+(t) = P_+(0)\exp(i\gamma_\mu\langle h\rangle t)\exp\left(i\gamma_\mu \int_0^t \delta h(\tau)\,d\tau\right). \tag{4.21'}$$

Expanding the second exponential in (4.21) in a series we retain only the linear and the quadratic terms. In the averaging over various realizations of $\delta h(t)$ only the quadratic term survives, and for the transverse polarization we have

$$P_\perp(t) = P_\perp(0)\left(1 - \gamma_\mu^2\langle\delta h^2\rangle \int_0^t d\tau \int_0^\tau d\tau_1 f(\tau-\tau_1)\right), \tag{4.22}$$

where $\langle\delta h^2\rangle f(\tau)$ is the autocorrelator of $\delta h(t)$.

Since $\tau_c \ll \tau_\mu$, we obtain, as usual

$$P_\perp(t) \approx P_\perp(0)e^{-\lambda t}, \tag{4.23}$$

where $\lambda = \gamma_\mu^2\langle\delta h^2\rangle\tau_c$ is the depolarization rate.

The Fourier spectrum of the polarization (4.23) has a Lorentzian shape, and hence the characteristic width can be taken as the half-width at half-maximum, $\Delta\omega_{1/2} = \lambda$, rather than the second moment. Therefore, if the spectrum has a

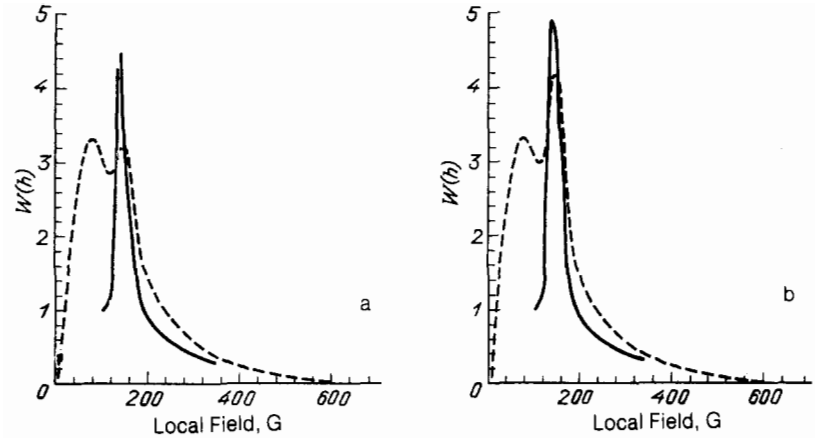

FIG. 11. Distribution function $W(h)$ for nonuniform creep. The case of "weak" pinning (solid line) and "strong" pinning (dashed line).

shape that is close to Lorentzian we can estimate the rate of creep as

$$V_c \approx \frac{\gamma_\mu^2 \langle \delta h^2 \rangle}{\Delta\omega_{1/2}} \left(\frac{\Phi_0}{H}\right)^{1/2}. \tag{4.24}$$

It is interesting to note that in the contraction that is obtained the difference between the external and internal field, $H_{ext} - \langle h \rangle$ remains unchanged. Of particular interest is the case of highly nonuniform pinning (for example in polycrystalline high-T_c superconductors), in which the creep can occur in places where the pinning is weak (for example along the intergranular region; see Section 5). Although there is no creep in the rest of the sample, the sample acquires a finite resistance. Clearly, the Fourier spectrum of the polarization is the sum of the spectra from the mobile and the immobile "sublattices." The characteristic shapes of such spectra is shown in Fig. 11.

Let us turn now to "slow" creep. We shall first consider a sub-ensemble of muons with a given value of the field at the initial moment of time. The local field $h(t)$ is

$$h(t) = h_0 + V_\alpha^i \nabla_\alpha h(\mathbf{r}^i) + \frac{1}{2} V_\alpha^i V_\beta^j \nabla_\alpha h(\mathbf{r}^i) \nabla_\beta h(\mathbf{r}^j), \tag{4.25}$$

where V_α^i is the αth component of the velocity of the ith vortex, $\mathbf{r}^i$ is the coordinate of the ith vortex, and the summation convention is understood for pairs of indices.

If we substitute (4.25) into (4.21) we obtain with an accuracy to the first significant terms

$$P_+(t) = P_+(0) \exp\left[i\gamma_\mu \left(h_0 t + \langle V_c^2 \rangle \langle \Delta h \rangle_0 \frac{t^3}{6}\right)\right] \times \left(1 - \gamma_\mu^2 \langle V_c^2 \rangle \sum_i \langle \mathrm{grad}^2 h(\mathbf{r}^i) \rangle_0 \frac{t^4}{4}\right), \tag{4.26}$$

where the averages $\langle \mathrm{grad}^2 h(\mathbf{r}^i) \rangle_0$ and $\langle \Delta h \rangle_0$ are taken over the isolines of h_0:

$$\Delta h \equiv \left(\frac{\partial^2}{\partial x^2} + \frac{\partial^2}{\partial y^2}\right) h,$$

$$\Delta h = \sum_i \Delta h(\mathbf{r}^i);$$

and $\langle \Delta h \rangle = \lambda^{-2} h_0$ over the entire volume of the sample except the core.

In this way we can find $P(\omega, h_0)$, the spectrum of the sub-ensemble of muons for which the field at the initial time is equal to h_0. The complete spectrum is obtained from a convolution of $P(\omega, h)$ with the field distribution in the absence of creep.

A detailed analysis is extremely tedious, and so we offer only the conclusions. "Slow" creep leads to a smoothing of the spectrum (different for different frequencies) and to a nonuniform compression in frequencies, proportional to $\langle V_c^2 \rangle$. There is a natural separation of the cases of strong and weak pinning. For strong pinning the available information on creep can be obtained from the second moment, but the case of weak pinning is more informative. Averaging along the isolines can be carried out numerically, and in addition to the second moment, the smoothing of the spectrum at the singular points can also provide interesting information.

5. EXPERIMENTAL STUDIES OF THE VORTEX LATTICE OF HIGH-T_c SUPERCONDUCTORS

In experiments on the vortex structure of high-T_c superconductors by the μ SR method the following method is usually used: The field cooling (FC) method, in which the sample undergoes the superconducting transition under an external magnetic field H_{ext} which is applied when the temperature is above the critical point, and zero-field cooling (ZFC), in which the sample goes into the superconducting state in zero field and then the field is turned on at $T < T_c$. The experiments are carried out in a transverse, $\mathbf{H}_{ext} \perp \mathbf{P}(t=0)$, as well as in a longitudinal, $\mathbf{H}_{ext} \| \mathbf{P}(t=0)$, magnetic field.

To estimate the penetration depth λ one ordinarily uses the second moment of the distribution of fields in the vortex lattice. The calculation of the second moment is still the only procedure for determining λ for a superconductor with the use of the Fourier spectrum $P(\omega)$. In Sections 2 and 3 we formulated a method based on the determination of the positions of the Van Hove singularities.

In the London limit the second moment in units of the muon frequency is

$$\langle \Delta\omega^2 \rangle = \langle \omega \rangle^2 - \langle \omega^2 \rangle = \gamma_\mu^2 B^2 \sum_{\mathbf{k}}' (1 + \lambda^2 \mathbf{k}^2)^{-2}, \tag{5.1}$$

where the summation Σ' is taken over all the vectors $\mathbf{k} \neq 0$ of the reciprocal lattice. As can be seen, $\langle \Delta\omega^2 \rangle$ contains sufficient information to determine λ. Replacing the summation with an integration for $a \gg \lambda$ yields the well-known approximate formulas (see, e.g., Ref. 4)

$$\langle \Delta\omega^2 \rangle = \gamma_\mu^2 B^2 \left\{ 4\pi \left(\frac{\lambda}{a}\right)^2 \left[1 + 4\pi^2 \left(\frac{\lambda}{a}\right)^2 \right] \right\}^{-1} \tag{5.2a}$$

for a square lattice, and

$$\langle \Delta\omega^2 \rangle = \gamma_\mu^2 B^2 \left\{ 2\sqrt{3}\,\pi \left(\frac{\sqrt{3}\lambda}{2a}\right)^2 \left[1 + 4\pi^2 \left(\frac{\sqrt{3}\lambda}{2a}\right)^2 \right] \right\}^{-1} \tag{5.2b}$$

for a triangular lattice.

As can be seen, when $a \ll \lambda$ (an intermediate field) the second moment $\langle \Delta\omega^2 \rangle$ is independent of the applied field:

$$\langle \Delta\omega^2 \rangle = (16\pi^3)^{-1} \left(\frac{\gamma_\mu \Phi_0}{\lambda^2}\right)^2 \approx 0{,}00201 \left(\frac{\gamma_\mu \Phi_0}{\lambda^2}\right)^2 \tag{5.3a}$$

for a square lattice, and

$$\langle \Delta\omega^2 \rangle = \sqrt{3}\,(32\pi^3)^{-1} \left(\frac{\gamma_\mu \Phi_0}{\lambda^2}\right)^2 \approx 0{,}00175 \left(\frac{\gamma_\mu \Phi_0}{\lambda^2}\right)^2 \tag{5.3b}$$

for a triangular lattice.

In general, going over to an integration entails substantial errors, and it is simpler to sum directly the series (5.1), which converges quite rapidly (see, e.g., Ref. 43). The summation of even the first terms shows that the formulas for the second moment (5.3) greatly underestimate it. An exact calculation yields the result[43]

$$\langle \Delta\omega^2 \rangle \approx 0{,}00386 \left(\frac{\gamma_\mu \Phi_0}{\lambda^2}\right)^2 \tag{5.4a}$$

for the square lattice, and

$$\langle \Delta\omega^2 \rangle \approx 0{,}00371 \left(\frac{\gamma_\mu \Phi_0}{\lambda^2}\right)^2 \tag{5.4b}$$

for the triangular lattice.

Fortunately, the second moment $\langle \Delta\omega^2 \rangle$ is proportional to λ^{-4}, and so even though the numerical coefficients in (5.3) are underestimated by almost a factor of two, their use only results in at most a 20% error in the determination of λ.

The results of the calculations for the two types of lattices are shown in Fig. 12. It can be seen that, depending on the external field H_{ext} (the induction B), we have three regions. For small fields, $H_{c1} \lesssim H_{ext} \ll H_{c2}$, the second moment increases with B, and the dependence of $\langle \Delta\omega^2 \rangle$ on B is given by formulas (5.2).

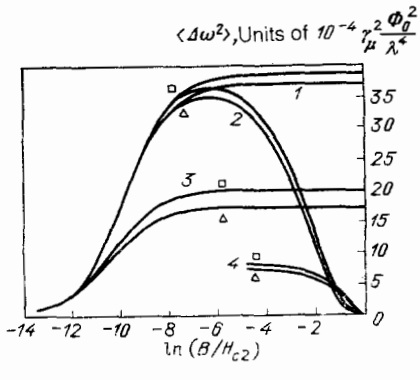

FIG. 12. Second moment $\langle \Delta\omega^2 \rangle$ of the Fourier spectrum, calculated by different methods for square and triangular vortex lattices ($\varkappa = 70$); *1*) Lattice of London vortices (5.1); *2*) the vortex core approximated by a Gaussian of width ξ (5.6); *3*) summation replaced by an integration (5.2); *4*) for an Abrikosov lattice (5.5).

For the case of intermediate fields, $H_{c1} \ll H_{ext} \ll H_{c2}$, the second moment is practically independent of the applied field and formulas (5.4) are applicable. The further decrease in $\langle \Delta\omega^2 \rangle$ with increasing H_{ext} is related to the overlapping of the cores of the vortices. Using the solution of the Ginsburg–Landau equations for the case $H_{ext} \lesssim H_{c2}$ (2.5) we find[43]

$$\langle \Delta\omega^2 \rangle \approx 0{,}000944 \left(\frac{\gamma_\mu \Phi_0}{\lambda^2}\right)^2 \left(1 - \frac{B}{H_{c2}}\right)^2 \tag{5.5a}$$

for the square lattice, and

$$\langle \Delta\omega^2 \rangle \approx 0{,}000819 \left(\frac{\gamma_\mu \Phi_0}{\lambda^2}\right)^2 \left(1 - \frac{B}{H_{c2}}\right)^2 \tag{5.5b}$$

for the triangular lattice.

Within the London approximation, representing the core of a vortex by a Gaussian of width ξ, we obtain an approximate expression for the second moment, which is valid in a wide range of fields[44]

$$\langle \Delta\omega^2 \rangle = \gamma_\mu^2 B^2 \sum_{\mathbf{k}}{}' (1 + \lambda^2 \mathbf{k}^2)^{-2} e^{-\mathbf{k}^2\xi^2}. \tag{5.6}$$

We note that formulas (5.4) and (5.5) remain valid for orientations $\mathbf{H}_{ext} \| \mathbf{c}$ and $\mathbf{H}_{ext} \perp \mathbf{c}$ for an anisotropic superconductor. It is necessary only to make the substitution $\lambda^2 \to \lambda_{ab}^2$ in the case $\mathbf{H}_{ext} \| \mathbf{c}$ and $\lambda^2 \to \lambda_{ab}\lambda_c$ in the case $\mathbf{H}_{ext} \perp \mathbf{c}$.

We recall that the width (second moment) of the Fourier spectrum $P(\omega)$ results not only from the distribution of fields of the vortex lattice, but also from the interaction with the magnetic fields of the nucleus (dipole and quadrupole interactions). The characteristic broadening due to the nuclear dipole and quadrupole interactions is $\langle \Delta\omega^2 \rangle^{1/2} \approx 2 \cdot 10^5$ to $10^6\,\mu s^{-1}$, whereas the broadening due to the nonuniformity of the field, according to formulas (5.4) in intermediate fields with $\lambda = 1000$ Å is $\langle \Delta\omega^2 \rangle^{1/2} \approx 10^7\,\mu s^{-1}$, while for $\lambda = 3000$ Å it is $\langle \Delta\omega^2 \rangle^{1/2} \approx 1.2 \cdot 10^6\,\mu s^{-1}$. Thus, the distortion of the second moment of $P(\omega)$ may be more pronounced in superconductors with $\lambda \gtrsim 3000$ Å. This is particularly true in the case of anisotropic high-T_c superconductors with the orientation $\mathbf{H}_{ext} \perp \mathbf{c}$ (for $YBa_2Cu_3O_7$, $[\lambda_{ab}\lambda_c]^{1/2} \approx 3250$ Å). The nuclear broadening mechanism has no effect on the position of the Van Hove singularities in $P(\omega)$, and therefore the method that is based on the determination of the characteristic frequencies is more reliable.

In the majority of the experiments to the present time the second moment has been determined incorrectly. Specifically, the time dependence of the polarization has been approximated by a Gaussian or exponential relaxation

$$P_G(t) \propto e^{-t^2\sigma^2}, \tag{5.7a}$$

$$P_e(t) \propto e^{-t\sigma}. \tag{5.7b}$$

The second moment of a Gaussian relaxation has the form

$$\langle \Delta\omega^2 \rangle_g = 2\sigma^2. \tag{5.8}$$

In the case of an exponential relaxation the Fourier spectrum is $P_e(\omega) \propto \sigma[\sigma^2 + (\omega - \langle\omega\rangle)^2]^{-1}$ (the Lorentzian line shape). In this case the second moment is undefined, and one ordinarily uses the quantity $\Delta\omega_e = \sqrt{2}\,\sigma$ as the "halfwidth" of the spectrum. However, as we have seen (Fig. 3), there does not in general exist a spectrum of an

ideal vortex lattice that is either Gaussian or Lorentzian. Therefore, fitting $P(t)$ with curves (5.7) and then interpreting the quantity $2\sigma^2$ as the second moment of the spectrum is incorrect. This can be seen even from the fact that for various choices for the approximation to $P(t)$ for the same experimental data we find a considerable spread in the second moment: from a finite value for a Gaussian to infinity for the exponential decay. Accordingly, this situation leads to error in the determination of $P(t)$. The correct method of analyzing the experimental data involves the determination of $\langle\Delta\omega^2\rangle$ directly from the Fourier spectrum $P(\omega)$ (and not from $P(t)$). Henceforth we shall use formulas (5.4) for the determination of λ.

It has been shown rather recently[45] that in the case of a polycrystalline sample the fitting of the experimental data $P_{\exp}(t)$ by means of curves with a Gaussian relaxation (5.7a) results in relatively small errors in the determination of the second moment $\langle\Delta\omega^2\rangle$. Pümpin *et al.*,[45] used untextured polycrystalline samples of $YBa_2Cu_3O_7$ ($H_{\text{ext}} = 3.5$ kG, $T = 10$ K, field-cooling). The experimental data were analyzed by four different methods:

a) fitting by a single Gaussian line $P_{\exp}(t) \to A\cos(\omega t)\exp(-\sigma^2 t^2) \to \langle\Delta\omega^2\rangle = 2\sigma^2$;

b) fitting by two Gaussian lines $P_{\exp}(t) \to A_1\cos(\omega_1 t) \times \exp(-\sigma_1^2 t^2) + A_2\cos(\omega_2 t)\exp(-\sigma_2^2 t^2) \to \langle\Delta\omega^2\rangle = 2\sigma_1^2$ (the signal that is proportional to A_2 is the interference due to muons that have stopped in the window of the cryostat and precess in the field H_{ext});

c) a numerical Fourier transformation $\operatorname{Re} F(P_{\exp}(t)) = P_{\exp}(\omega) \to \langle\Delta\omega^2\rangle$;

d) fitting $P_{\exp}(t)$ with a sum of sinusoidal functions $\Sigma_i A_i \cos(\omega_i t + \varphi)$, where ω_i and φ are specified and the Fourier components A_i are adjustable parameters.

The numerical calculation of the Fourier spectrum (c and d) for a polycrystalline sample showed that this spectrum is more symmetrical than in the case of an ideal vortex lattice in a single crystal, and in its shape it is reminiscent of a Gaussian. This result may be due to strong pinning (Section 4, Fig. 8) or may be an artifact of the summation over granules of various orientations. Therefore, systematic errors associated with methods a) and b) are relatively small. The values of $\langle\Delta\omega^2\rangle^{1/2}$ obtained by methods a)–d) differ from their mean value by 4–7%, which is an estimate of the corresponding systematic errors. Thus, the use of a Gaussian relaxation in the fitting is partially justified. It should be emphasized that the results obtained in Ref. 45 are for untextured polycrystalline samples.

The great majority of experiments, as we remarked previously, have been conducted with polycrystalline samples (high-T_c ceramics). The "isotropic" values of λ that have been obtained for polycrystalline high-T_c superconductors are in fact some sort of average characteristics λ_{eff} over the sample. For granules that are oriented with $\mathbf{c}\|\mathbf{H}_{\text{ext}}$ the second moment is $\langle\Delta\omega^2\rangle \propto \lambda_{ab}^{-4}$, and for the orientation $\mathbf{c}\perp\mathbf{H}_{\text{ext}}$ it is $\langle\Delta\omega^2\rangle \propto (\lambda_{ab}\lambda_c)^{-2}$. Therefore, the estimate of λ from formulas (5.4) for an isotropic superconductor gives in the first case the value λ_{ab} and in the second $(\lambda_{ab}\lambda_c)^{1/2} = \lambda_{ab}(1+\chi)^{1/4}$. For $YBa_2Cu_3O_7$ these numbers differ by more than a factor of two, and for $(LaSr)_2CuO_4$ by almost a factor of four.[6] Incorrect analysis of the experimental data can thus lead to a severalfold error in the determination of λ.

A simple estimate of the second moment $\langle\Delta\omega^2\rangle$ and some features of the Fourier spectrum for polycrystalline samples can be obtained for intermediate fields $H_{\text{ext}} \gg H_{c1}^c$.

In this approximation, the vectors $\mathbf{H}_{\text{ext}}$, $\mathbf{B}$, and $\mathbf{h}(\mathbf{r})$ are parallel to each other within a small angle for any orientation of the single crystal in the magnetic field. Here $\mathbf{H}_{\text{ext}}$ and $\mathbf{B}$ are related by (see, e.g., Ref. 21)

$$\mathbf{H}_{\text{ext}} \approx \mathbf{B} + \frac{\Phi_0}{4\pi\lambda_{ab}^2} g(\theta) \ln\left(\frac{H_{c2}(\theta)}{H_{\text{ext}}}\right)^{1/2} \mathbf{n}_{\|}, \tag{5.9}$$

where $\theta = \mathbf{B}\hat{}\mathbf{c}$, $g(\theta) = [(1+\chi\cos^2\theta)/(1+\chi)]^{1/2}$, $H_{c2}(\theta) = \Phi_0/(2\pi\xi_{ab}^2 g(\theta))$, and $\mathbf{n}$ is a unit vector parallel to $\mathbf{B}$.

The microscopic field in the vortex lattice of an anisotropic high-T_c superconductor can be written in the form

$$\mathbf{h}(\mathbf{r}) = B[\delta h_x(\mathbf{r})\mathbf{x} + \delta h_y(\mathbf{r})\mathbf{y} + (1+\delta h_z(\mathbf{r}))\mathbf{z}]. \tag{5.10}$$

It can be shown that the scale of variation of $\delta h_{x,y,z}$ in no case exceeds $2H_{c1}^c/B$, and the average over the cell of the lattice is $\langle\delta h_{x,y,z}\rangle = 0$. The quantity $\gamma_\mu h$ is proportional to $(1-\delta h_x^2)/\langle 1-\delta h_x^2\rangle$ (we assume that the initial polarization is $\mathbf{P}(0)\|\mathbf{x}$ and the axis of observation is the x axis). Up to terms of order $[2H_{c1}^c/B]^2$ we have

$$h^2 = B^2[\delta h_x^2 + \delta h_y^2 + (1+\delta h_z)^2],$$
$$h \approx B\left(\frac{\delta h_x^2}{2} + \frac{\delta h_y^2}{2} + 1 + \delta h_z\right). \tag{5.11}$$

From this it can be seen that the effect of the transverse (x and y) components of the field on the Fourier spectrum can be neglected in comparison to the effect of the longitudinal, z component (with an accuracy to $\sim H_{c1}^c/H_{\text{ext}}$). In this case the distribution of the fields and the Fourier spectrum coincide, and, clearly, they have a single Van Hove singularity. (The nonequivalence of the saddle points of the function $h(x,y)$ shows up only in considerations of the transverse components of the field, $\Delta\omega_{\text{sad}} \propto 1/B$.)

For a correct determination of the second moment of the spectrum $\langle\Delta\omega^2\rangle \propto (H_{c1}^c/H_{\text{ext}})^2$, we shall carry out calculations, retaining in formulas (5.11) the transverse components of $\mathbf{h}$:

$$\langle\omega^2\rangle = \gamma_\mu^2 B^2 \langle h^2(1-\delta h_x^2)\rangle\langle 1-\delta h_x^2\rangle^{-1}$$
$$= \gamma_\mu^2 B^2(1 + \langle\delta h_x^2\rangle + \langle\delta h_y^2\rangle + \langle\delta h_z^2\rangle),$$
$$\langle\omega\rangle = \gamma_\mu B\langle h(1-\delta h_x^2)\rangle\langle 1-\delta h_x^2\rangle^{-1} \tag{5.12}$$
$$= \gamma_\mu B\left(1 + \frac{\langle\delta h_x^2\rangle}{2} + \frac{\langle\delta h_y^2\rangle}{2}\right).$$

Ultimately, we find that $\langle\Delta\omega^2\rangle$ in this approximation is determined by the z component:

$$\langle\Delta\omega^2\rangle = \langle\omega^2\rangle - \langle\omega\rangle^2 = \gamma_\mu^2 B^2\langle\delta h_z^2\rangle. \tag{5.13}$$

A calculation of the field in the vortex lattice of an anisotropic high-T_c superconductor is carried out with the use of formulas (3.7). Assuming that $\alpha^2 \ll 1$ for $H_{\text{ext}} \gg H_{c1}$, we rewrite the expression for h_z as

$$h_z = B + \frac{\Phi_0}{4\pi\lambda_{a,b}^2} g(\theta) \sum_{n,m}{}' \frac{\exp[2\pi i(n\tilde{x} + m\tilde{y})]}{n^2 + m^2\tau'^2}, \tag{5.14}$$

where $\tau' = (a/b)g(\theta)$. It can be seen that when the replacement $\tau' \to \tau$ is made formula (5.14) coincides with (1.13) for an isotropic superconductor ($\alpha^2 \ll 1$). Accordingly, by analogy with the isotropic case we have a minimum in the free energy for $\tau' = 1$ (for the rectangular lattice) and for $\tau' = 1/\sqrt{3}$ (for the triangular lattice).

The expressions for h_z (5.14) for various angles θ differ only by the factor $g(\theta)$. The corresponding field distribution is obtained by a change in scale. In particular,

$$\omega_{\min(\mathrm{sad})}(\theta) - \langle\omega\rangle = (\omega_{\min(\mathrm{sad})}(0) - \langle\omega\rangle)\, g(\theta), \qquad (5.15)$$
$$\langle\Delta\omega(\theta)^2\rangle = \langle\Delta\omega(0)^2\rangle\, g(\theta)^2,$$
$$P(\tilde{\omega}, \theta) = \frac{P(\tilde{\omega}/g(\theta), 0)}{g(\theta)},$$

where $\tilde{\omega} = (\omega - \langle\omega\rangle)/\langle\omega\rangle$, $P(\tilde{\omega},\theta)$ is the field distribution (the Fourier spectrum) in the vortex lattice, and $\omega_{\min}(0)$, $\omega_{\mathrm{sad}}(0)$, and $\langle\Delta\omega(0)^2\rangle$ are given by formulas (3.10) and (5.4).

The formulas that have been obtained can be used to describe the Fourier spectrum of polycrystalline high-T_c superconductors. However, it is necessary to stipulate a model for the distribution of the magnetic field over the granules of the polycrystalline sample. The case that is usually considered is the most simple one, where $\mathbf{B}(\mathbf{r})$ is a constant over the sample and is uniform at the boundaries of the granules. ($\mathbf{B}(\mathbf{r}) = \langle\mathbf{h}\rangle$, the local induction, averaged over a region of dimensions of the order of the unit cell of the vortex lattice). The density of vortex filaments is taken to be the same over the entire granule, the geometry of the vortex lattice depends on the orientation of the **c** axis of the granule, and the effect of the distortion of the vortex filaments at the boundaries of the granules is ignored. The construction of a model for the behavior of the field in a polycrystalline material is attended with considerable complexities (the necessity to take into account the geometry of the granules, the nonuniformities of the field in the granules, and other factors).

The results of averaging of the second moment of the spectrum over all equal-probability orientations of the **c** axis of the granules of the polycrystalline sample for this model are

$$\langle\Delta\omega^2\rangle_{\mathrm{pol}} = \langle\Delta\omega(0)^2\rangle(3+\chi)[3(1+\chi)]^{-1}. \qquad (5.16)$$

When χ is large, $\chi \gg 1$, formula (5.16) for a triangular lattice becomes

$$\langle\Delta\omega^2\rangle_{\mathrm{pol}} = \frac{1}{3}\langle\Delta\omega(0)^2\rangle = \frac{1}{3}\,3{,}71\cdot 10^{-3}\left(\frac{\gamma_\mu\Phi_0}{\lambda_{ab}^2}\right)^2. \qquad (5.17)$$

Thus, in the case of a strong anisotropy the second moment of the Fourier spectrum is expressed only in terms of λ_{ab}. Formula (5.17) can be used to estimate λ_{ab} in a μ SR experiment if it is known *a priori* that $\lambda_\chi \gg \lambda_{ab}$.

The discrepancy between the result (5.17) and the data of numerical calculations[46] comes about because the authors of Ref. 46 actually averaged the quantity

$$\langle\Delta\omega^2\rangle + \langle\omega\rangle^2 - \gamma_\mu^2 B^2 = \gamma_\mu^2 B^2(\langle\delta h_x^2\rangle + \langle\delta h_y^2\rangle + \langle\delta h_z^2\rangle), \qquad (5.18)$$

(see (5.12)), which is an overestimate of the second moment. Therefore, the expression for λ_{eff} in Ref. 46 needs correction; namely:

$$\lambda_{\mathrm{eff}} = 3^{1/4}\lambda_{ab} \approx 1{,}32\,\lambda_{ab} \qquad (5.19)$$

which is the effective penetration depth for a polycrystalline sample as determined from the second moment of the Fourier spectrum according to the formulas for an isotropic superconductor (5.4) under the condition $\chi \gg 1$. We emphasize that because of the arbitrariness of the model used, the distributions of the fields over the granules in formulas (5.17) and (5.19) are only rough estimates.

In the analysis of the experimental data, most investigations do not take into account the disruption of the ideal representation of the vortex lattice and of the field distribution due to pinning. In granular samples containing defects it is obvious that these distortions must be very important. Because of pinning, thermodynamic equilibrium of the state of the high-T_c superconductor is not attained in the sample. This fact is unambiguously demonstrated by the difference between the results of field-cooled and zero-field-cooled experiments and the observation of hysteresis phenomena. In this connection we should mention in particular the work reported in Ref. 47, where substantial magnetic fields were observed to be frozen in; that is, residual fields remained in the superconductor after the external field H_{ext} was turned off. It is quite clear that all these properties of the vortex lattice and, correspondingly, of the Fourier spectrum $P(\omega)$ refer to the equilibrium states of the superconductor. In the conduct of the experiments it is essential to monitor the departure from equilibrium of the sample studied.

The first systematic and extremely important investigations of the equilibrium and nonequilibrium states of high-T_c superconductors were carried out in Refs. 42 and 48. Pümpin *et al.*,[48] measured the average muon precession frequency ν_μ and the rate of depolarization σ as functions of the temperature for a ceramic sample of $YBa_2Cu_3O_7$. Both the FC and the ZFC processes were studied. The data obtained (Fig. 13) indicate the irreversible behavior of the sample prepared by zero-field cooling at temperatures $T < T^*$, and the reversibility in the case of field cooling at any temperature. The irreversible behavior in the case of ZFC is an indication of the pinning-induced nonequilibrium nature of the state of the vortex lattice in the superconductor. As the temperature is increased, vortices are detached from the pinning centers, and the degree of equilibrium increases as the lattice

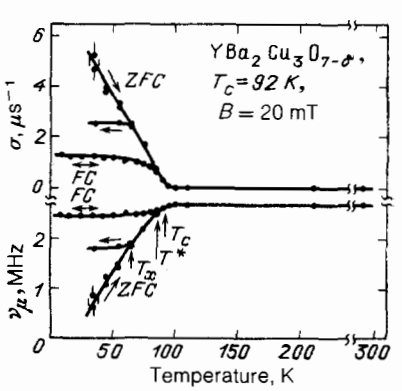

FIG. 13. Muon precession frequency ν_μ and rate of depolarization σ as functions of the temperature ($H_{\mathrm{ext}} = 2$ kG; ceramic sample of $YBa_2Cu_3O_7$, field-cooled (FC) and zero-field-cooled (ZFC) (Ref. 48).

becomes more regular. The temperature T^* is close to T_c and corresponds to the complete detachment of the vortices from the pinning centers for a given value of B ($T^*(0) - T^*(B) \propto B^{2/3}$). For $T > T^*$ the states that are obtained with field cooling and those obtained with zero-field cooling are identical.

The effect of a dc current on the vortex lattice in high-T_c superconductors (ceramic samples of $YBa_2Cu_3O_7$) has been studied in Ref. 42. Figure 14 shows the experimentally determined curves of $\nu_\mu(I)$ and $\sigma(I)$ for the case of ZFC and FC. These curves show that for the state prepared by the FC procedure the relaxation rate and the average precession frequency do not depend on the current in the sample. Those workers showed that the observed pattern is reversible when a current is flowing (Fig. 14), where the maximum current $j = 40$ A/cm^2 exceeded the critical current in the sample, $j_c \approx 34$ A/cm^2. These results show quite convincingly that the vortex lattice that is formed in the field-cooled process is in equilibrium. Contrarily, for the zero-field-cooled case, either with a current passing, or with variation in sample temperature, its behavior is markedly irreversible. This situation corresponds to the detachment of the vortices from the pinning centers under the action of the Lorentz force generated by the electric current. Here the current passes with the dissipation of energy, which is manifested in an increase in the resistance. The critical current I_c, indicated in Fig. 14, is measured by a sharp increase in the voltage drop in the circuit. Pümpin *et al.*, hypothesized that this current corresponds to the intergranular current (j_c), which is some 10^2 to 10^3 times lower than the intragranular "true" critical current j^g_c. Therefore, even for $j > j_c$ the superconducting state remains within the granules and the distribution of the magnetic fields in the vortex lattice is virtually unchanged.

We should also mention the interesting results of Ref. 42, in which it is demonstrated that flux is captured in the superconductor after the magnetic field is turned off abruptly (field-cooled, $H_{ext} = 1$ kG, $T = 20$ K, polycrystalline $YBa_2Cu_3O_7$). The envelope of the distribution of the internal fields (Fig. 15a) resembles the distribution in the case of

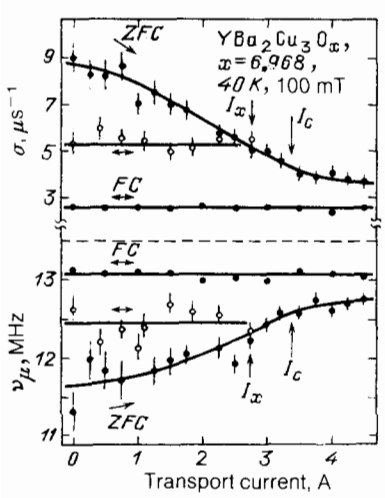

FIG. 14. Muon precession frequency ν_μ and rate of depolarization σ as functions of the current ($H_{ext} = 10$ kG, $T = 40$ K, ceramic sample of $YBa_2Cu_3O_7$, FC and ZFC). The dashed line corresponds to the precession frequency in the field H_{ext} (Ref. 42).

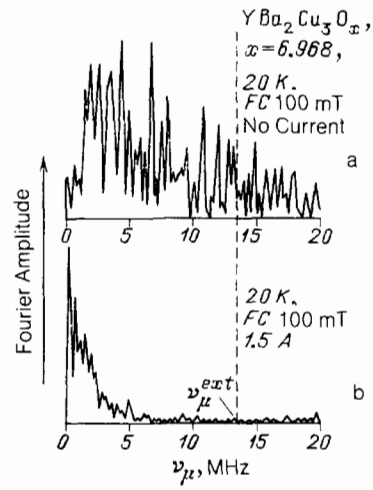

FIG. 15. μ SR spectrum of a sample with trapped flux (ceramic sample of $YBa_2Cu_3O_7$, $H_{ext} = 10$ kG, FC, $T = 20$ K) after rapid turn-off of the field. a) No current; b) current of 1.5 A. The dashed line corresponds to the precession frequency in the field H_{ext} (Ref. 42).

a random vortex lattice with strong pinning (Section 4, Fig. 8). The sharp peaks in the distribution can be interpreted as being the result of local order in a random vortex structure of the superconductor. When a dc current flows, much of the flux is expelled from the sample (Fig. 15b). The expulsion of the flux is observed already at a current $j = 1.6$ A/cm^2, which is very low compared to j_c. This fact appears to indicate that the expulsion is related to the detachment of weak pinning at the intergranular interfaces. It is not understood, however, in what way the vortices are detached from the strong pinning centers within the granule. In accordance with the Bean–Anderson models we can propose that the density of pinning centers near the surface of a granule is much higher than in the bulk, but the "force" of surface pinning is highly anisotropic, and for the motion of a vortex along the surface it is considerably less than for motion in the interior or for the bulk centers. In zero applied field expulsion of the surface vortices from the sample is possible along the intergranular boundaries even for a small current. Here the equilibrium of the bulk lattice is unavoidably disrupted, and strong forces arise that force the vortices to the surface of the granule, from which they are again removed by the current. However, at present only the first results have been obtained, and therefore it is premature to presume that the interpretation is reliable. The pioneering experiments of Ref. 42 should be repeated with single crystal samples. We emphasize that the μ SR experiments under conditions of current flow are of extreme interest, not only for high-T_c superconductors but also in that they open up completely new possibilities for the study of the pinning and creep of flux in technological superconductors.

Estimates of the penetration depth λ, made in various investigations for various high-T_c superconductors are listed in Table I. As a rule, the temperature dependence $\lambda(T)$, formula (1.6), is experimentally verified, and the listed values of $\lambda(0)$ are the result of extrapolation to $T = 0$. Because of the features of the experiments noted above, and because the experimental data were analyzed improperly, the values listed can be regarded only as qualitative estimates. This conclusion is also supported by the large spread in the results

obtained by the various investigators.

The first investigations of the vortex lattice in $La_{1.85}Sr_{0.15}CuO_4$ ceramics were carried out in the work reported in Refs. 49 and 50. The measured value of λ at $T = 6$ K (ZFC) was 2300 Å. The temperature dependence, $\lambda(T)$, differed from that predicted by formula (1.6), and this discrepancy was explained by the nonuniformity of the high-T_c sample. Measurements made in longitudinal fields indicate that there are transverse components in the microscopic field in the sample, and these are due to pinning and anisotropy. The investigators note the presence of hysteresis in the rate of polarization relaxation, which depends on the history of the sample. Experiments on $La_{1.85}Sr_{0.15}CuO_4$ (Refs. 51, 52) yield good agreement with the temperature dependence $\lambda(T)$ given by formula (1.6). The values of λ extrapolated to $T = 0$ are 2650 Å and 2300 Å, respectively.

In studies of the $YBa_2Cu_3O_7$ ceramic,[53,54] the results of averaging[46] were used to estimate the value of λ_{ab} (see Table I).

Schenck[55] has taken into account the distortion of the regularity of the vortex lattice due to the granular structure of the high-T_c ceramic. In the polarization of the ensemble of muons, these investigators distinguished two components, each of which is characterized by its own amplitude, oscillation frequency, and relaxation rate. The "fast" component (with a high relaxation rate) is presumably related to a region of the sample in which the granules are randomly oriented. The "slow" component is related, the authors believe, to regions in which the vortex lattice is regular, i.e., the granules are ordered (there is a preferred orientation of the c axis). Thus, the analysis of the slow component yields information on the penetration depth λ. The investigators[53–55] concluded that the predominant orientation of the granules was $\mathbf{c} \perp \mathbf{H}_{ext}$, and estimated λ_c: $\lambda_c(0) \geqslant 6000$ Å for $YBa_2Cu_3O_7$ and $\lambda_c(0) >$ for $La_{1.85}Sr_{0.15}CuO_4$. The two components of $P(t)$ also have been reported in Refs. 56 and 57.

A detailed investigation has been made[47] of the penetration of the magnetic field into a sample during magnetization (zero-field cooling). The general features of the field penetration were obtained with the integrated method. This method is based on the measurement of the integrated counting rate of decay positrons

$$n_e = \int_0^{\Delta t} n(t)\,dt \quad (\Delta t \approx 10^{-5}\,\text{c}) \tag{5.20}$$

as a function of the external field and of the temperature, and from it one can draw qualitative conclusions about the processes taking place in the superconductor. In particular, Barsov *et al.*[47] note that the penetration of the field into the sample proceeds in two stages at temperatures $T < 60$ K. The proposed interpretation of this phenomenon is, however, quite arbitrary: In the first stage, according to the authors, the magnetic field penetrates into the intergranular space at $H_{ext} = H_1$ ($H_1 < H_{c2}$), and as the external magnetic field is further increased the field penetrates from the intergranular space into the granule near H_{c1}. The investigators[47] were not able to explain by means of this model the properties of the "intergranular" field in the range $H_{c1} < H_{ext} < H_{c1}$, where the integrated count rate was essentially independent of H_{ext}.

The most reliable results are those reported in Ref. 24 by Harshman *et al.*, who used the muon method to study $YBa_2Cu_3O_7$ single crystals. They postulated the following form of the Fourier spectrum $P(\omega)$:

$$\begin{aligned} P(\omega) &= (\omega_0^{-1} \exp[-(\omega - \omega_c)/\omega_0] \quad &\text{for } \omega \geqslant \omega_c, \\ &= 0 &\text{for } \omega < \omega_c, \end{aligned} \tag{5.21}$$

where ω_c corresponds to the minimum field in the vortex lattice, while the maximum field (in the vortex core) is taken to be infinite ($\xi \to 0$). The assumed shape of the spectrum (5.21) is different from the theoretical shape, but it describes the field distribution in an ideal lattice more accurately than a Gaussian or a Lorentzian does. To determine λ we used the formula for the second moment $\langle \Delta\omega^2 \rangle = \omega_0^2$. For a field direction $\mathbf{H}_{ext} \| \mathbf{c}$ we derived the value $\lambda_{ab} = 1430$ Å. Measurements carried out with other field directions gave the estimate $\lambda_c \geqslant 7000$ Å.

Investigations of high-T_c ceramic superconductors based on Y, La, Bi, and Tl have been reported in Ref. 59. For various stoichiometries measurements have been made of the critical temperature T_c and the muon depolarization rate $\sigma(T \to 0)$ in the mixed state of the superconductor (with the approximation of Gaussian relaxation (5.7a)). With increasing σ the critical temperature of the sample increases at first, and then it saturates and falls off. As has been shown experimentally, an initial increase in T_c is linear $T_c = \alpha\sigma(T \to 0)$, where α is a universal constant for all the superconductors studied. The temperature T_c at which saturation sets in, depends on the type of high-T_c superconductor. Uemura and his coworkers have interpreted the value of $2\sigma^2$ as the second moment of the Fourier spectrum (as we have seen for polycrystalline materials, this is only partially valid). Using formulas (5.17) in the case $\lambda_c \gg \lambda_{ab}$ and expression (3.5) for $\lambda_{\gamma\delta}$ we have

$$\sigma(T \to 0) \propto \frac{1}{\lambda_{ab}^2}(T \to 0) \propto \frac{n_s}{m_{ab}}, \tag{5.22}$$

where $n_s \propto |\psi_0|^2$ is the carrier concentration in the superconductor. Thus, we have the simple relation

$$T_c \propto \frac{n_s}{m_{ab}}, \tag{5.23}$$

which relates the critical temperature to the effective mass and the carrier concentration in the high-T_c superconductor. The general relation (5.23) has been corroborated in the experiments described in Refs. 60–62, while some discrepancies have been noted in Ref. 63. The curve $\sigma(T)$ in yttrium ceramic superconductors with various stoichiometric compositions have also been studied in Ref. 64.

Because it is difficult to prepare large single-crystal samples of high-T_c superconductors many investigators have used textured polycrystalline samples of superconductors[58,65,66] and packets (mosaics) of single crystals[67] to study the anisotropic properties of the superconducting state. In particular, a detailed study has been made[67] of the dependence of σ on the orientation of the sample (a mosaic of crystals) of $YBa_2Cu_3O_7$ and the temperature dependence of λ_c/λ_{ab} has been investigated[66] for a textured polycrystalline sample of this material. Barsov *et al.*[65] have estimated λ_{ab} and λ_c in $Bi_2Sr_2CaCuO_8$. Interesting investigations of

the mixed state in untextured high-T_c ceramics based on Gd and Bi have been carried out in Refs. 68 and 69.

6. LOCAL MAGNETIC FIELDS AND MAGNETIC ORDERING IN HIGH-T_c SUPERCONDUCTING COMPOUNDS

In a recent review[8] the magnetic properties of high-T_c compounds were analyzed, but the results of μ SR studies were hardly mentioned. Since μ SR experiments provide information that is inaccessible by neutron diffraction and NMR methods, it therefore appears timely to publish a review of investigations of the magnetic properties of high-T_c superconducting compounds by the μ SR method.

Before going on to the review, let us consider some features of the behavior of the muon spin polarization in antiferromagnets. Of course, the time dependence $\mathbf{P}(t)$ of the polarization is considerably different in single-crystal and polycrystalline materials. The most complete and clear-cut information is provided by experiments with single crystals. As can be seen from formulas (I.4)–(I.5) if the muon occupies equivalent sites in the magnetic lattice, it is possible to determine the local field $\mathbf{h}(\mathbf{r})$ at the muon.[1)] By carrying out experiments in external magnetic fields that differ in magnitude and direction one can also identify the location of the muon in the lattice.

Neutron diffraction experiments show that in high-T_c superconducting compounds there is collinear antiferromagnetism (see, e.g., Ref. 8). By studying single crystals by the muon method one can uniquely determine the magnetic structure independently and find the value of the internal magnetic field at the location of the muon.

The behavior of the muon spin polarization obviously depends to a large extent on whether or not the muon diffuses in the lattice. The experiments show that in high-T_c superconductors the muon begins to diffuse at a very high temperature ($T > 100$ K). Similar results were obtained in experiments with magnetic oxides (Fe_2O_3, Cr_2O_3, etc.) and rare-earth orthoferrites ($ReFeO_3$, where Re is a rare-earth element; see, e.g., Refs. 70–72). The orthorhombic lattice of these compounds is similar to that of the high-T_c superconductors. The following interpretation was advanced for the behavior of the muon in these compounds. The muon forms a complex M^{3+}–O^{2-}–μ^+ (Fig. 16), where M^{3+} is the trivalent metal ion.[70] The length of the muon-oxygen bond (O^{2-}–μ^+) is ≈ 1 Å. In the formation of such a complex a part of the spin density of the electrons in the complex are transferred to the muon, producing in the latter an additional contact field (see, e.g., Refs. 70, 73):

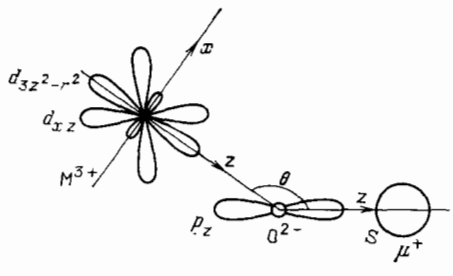

FIG. 16. Diagram of the complex M^{3+}–O^{2-}–μ^+

$$\mathbf{B}_{\text{cont}} = c \sum_a [(A_\sigma^2 - A_\pi^2)\cos^2\theta_a + A_\pi^2]\,\mathbf{n}_a, \tag{6.1}$$

where A_σ^2 and A_π^2 are the spin densities of the σ and π orbitals of the oxygen and $\mathbf{n}_a$ is the unit vector along the direction of the magnetic moment of the metal ion. The summation is taken over all the M^{3+}–O^{2-}–μ^+ complexes formed by the muon.

When the temperature is changed the muon that is bound in the M^{3+}–O^{2-}–μ^+ complex can change its position.[72] Accordingly, the local field at the muon changes because of the change in the dipole field and in the contact field (6.1).

The precession frequency of the polarization is completely determined by the modulus of the local field at the muon (I.4)–(I.5). If the muon can occupy interstitial sites with different local fields, a multifrequency pattern is seen.

Let us now consider the behavior of the polarization in magnetic polycrystalline materials, where the muon occupies interstitial sites having identical moduli of the internal local field. We assume that the muon does not diffuse. In formula (I.5) one must then average over equal-probability orientations of the time-independent internal field $\mathbf{h}_0(\mathbf{r})$ at the muon.[2)] In the absence of an external field the averaging is trivial, and we have

$$\mu_{\alpha\beta} = \left[\frac{1}{3} + \frac{2}{3}\cos(\omega t)\right]\delta_{\alpha\beta}. \tag{6.2}$$

Thus, 2/3 of the polarization precesses with the frequency $\omega = \gamma_\mu h_0$. Strictly speaking, the internal field at the muon cannot be regarded as static because of the contribution of the fluctuating magnetic field h_n created by the nuclear magnetic moment. Since $h_n \approx 1$ G, we should see a slow relaxation of the polarization with a rate $\Lambda \approx 10^5\ \text{s}^{-1}$.

In an external field $\mathbf{H}_{\text{ext}}$ the picture changes qualitatively.[3)] We shall examine two simple limiting cases: weak ($B \ll h_0$) and strong ($B \gg h_0$) external fields. We take the z axis parallel to $\mathbf{B}$. In both cases the precession frequency can be written as

$$\omega = \gamma_\mu |\mathbf{h}_0 + \mathbf{B}|$$
$$= \gamma_\mu (h_0^2 + B^2)^{1/2}[1 + h_0 B\cos\theta\,(h_0^2 + B^2)^{-1}] = \tilde{\omega} + \Omega\cos\theta, \tag{6.3}$$

where $\tilde{\omega} = \gamma_\mu (h_0^2 + B^2)^{1/2}$, and $\Omega = \gamma_\mu h_0 B (h_0^2 + B^2)^{-1/2}$. It can readily be seen that $\Omega \ll \tilde{\omega}$. Accordingly, the unit vectors are

$$n_z = \frac{h_{0z} + B}{(h_0^2 + B^2 + 2h_0 B\cos\theta)^{1/2}}$$
$$\approx \frac{h_0\cos\theta + B}{(h_0^2 + B^2)^{1/2}}\left(1 - \frac{h_0 B}{h_0^2 + B^2}\cos\theta\right), \tag{6.4a}$$

$$n_x = \frac{h_{0x}}{(h_0^2 + B^2 + 2h_0 B\cos\theta)^{1/2}}$$
$$\approx \frac{h_0\sin\theta\cdot\cos\varphi}{(h_0^2 + B^2)^{1/2}}\left(1 - \frac{h_0 B}{h_0^2 + B^2}\cos\theta\right). \tag{6.4b}$$

For an analysis of the muon experiments it is sufficient to consider two cases: a longitudinal ($\mathbf{B}\|\mathbf{P}(0)$) and a transverse ($\mathbf{B}\perp\mathbf{P}(0)$) field. In the longitudinal field only one of the components of the tensor (I.5) is nonzero:

$$\mu_{zz} = \frac{B^2 + (h_0^2/3)}{h_0^2 + B^2} - \frac{2h_0^2}{h_0^2 + B^2} \frac{\cos(\tilde{\omega}t)}{(\Omega t)^2} \left[\cos(\Omega t) - \frac{\sin(\Omega t)}{\Omega t}\right]$$
$$- \frac{2h_0^3 B}{(h_0^2 + B^2)^2} \frac{\sin(\tilde{\omega}t)}{(\Omega t)^2} \left\{\left[1 - \frac{3}{(\Omega t)^2}\right] \sin(\Omega t) + 3\frac{\cos(\Omega t)}{\Omega t}\right\}. \quad (6.5)$$

Correspondingly, $P_z(t) = \mu_{zz}(t)P(0)$, and $P_x(t) = P_y(t) = 0$.

As we can see, the oscillating component of the longitudinal polarization relaxes with a characteristic rate Ω. In a weak field we have $\Omega \approx \gamma_\mu B$, and for $B < 10$ G and an observation time $t < 1$ μs, formula (6.5) can be written approximately as

$$\mu_{zz} \approx \frac{1}{3} + \frac{2}{3}\left(1 - \frac{\Omega^2 t^2}{10}\right) \cos(\tilde{\omega}t) \approx \frac{1}{3} + \frac{2}{3}\cos(\tilde{\omega}t) \cdot e^{-\Omega^2 t^2/10}. \quad (6.6)$$

In a strong field the polarization $P_z(t)$ is quickly restored with a rate[4)] $\Omega \approx \gamma_\mu h_0$

$$\mu_{zz} \approx 1 - 2\left(\frac{h_0}{B}\right)^2 \frac{\cos(\tilde{\omega}t)}{(\Omega t)^2} \left[\cos(\Omega t) - \frac{\sin(\Omega t)}{\Omega t}\right]. \quad (6.7)$$

Let us examine now the case of transverse polarization. We take the x axis to be parallel to $\mathbf{P}(0)$. In this case the only nonzero component for an untextured polycrystalline sample is

$$\mu_{xx} = \frac{1}{3}\frac{h_0^2}{h_0^2 + B^2} + \frac{\cos(\tilde{\omega}t)}{\Omega t}$$
$$\times\left\{\sin(\Omega t) + \frac{h_0^2}{h_0^2 + B^2}\frac{1}{\Omega t}\left[\cos(\Omega t) - \frac{\sin(\Omega t)}{\Omega t}\right]\right\}$$
$$- \frac{2h_0^3 B}{h_0^2 + B^2} \frac{\sin(\tilde{\omega}t)}{(\Omega t)^2} \left\{\left[1 - \frac{3}{(\Omega t)^2}\right] \sin(\Omega t) + 3\frac{\cos(\Omega t)}{\Omega t}\right\}. \quad (6.8)$$

Correspondingly, $P_x(t) = \mu_{xx}(t)P(0)$ and $P_z(t) = P_y(t) = 0$.

In a weak field for "short" observation times we have

$$\mu_{xx} \approx \frac{1}{3} + \frac{2}{3}\left(1 - \frac{\Omega^2 t^2}{5}\right) \cos(\tilde{\omega}t) \approx \frac{1}{3} + \frac{2}{3}\cos(\tilde{\omega}t)\, e^{-\Omega^2 t^2/5}. \quad (6.9)$$

In a strong field the transverse polarization relaxes quickly practically to zero:

$$\mu_{xx} \approx \frac{1}{3}\left(\frac{h_0}{B}\right)^2 + \frac{1}{\Omega t}\cos(\tilde{\omega}t)\cos(\Omega t). \quad (6.10)$$

As can be seen from (6.10) the depolarization time is determined by the "spread" $\delta\mathbf{h}$ in the moduli of the local fields $|\mathbf{h} + \mathbf{B}|$ at the muon. In the present case the characteristic values are $\delta h \approx h_0$.

At low temperatures high-T_c ceramic superconductors transform into a magnetically ordered state. However, the magnetic properties of the ceramics $ReBa_2Cu_3O_x$ and La_2CuO_{4-y} ($(LaSr)_2CuO_4$) are different. We shall consider then separately. We note that practically all μ SR experiments have been performed with polycrystalline samples.

Antiferromagnetic ordering was first seen clearly in the non-superconducting tetragonal phase of the ceramic

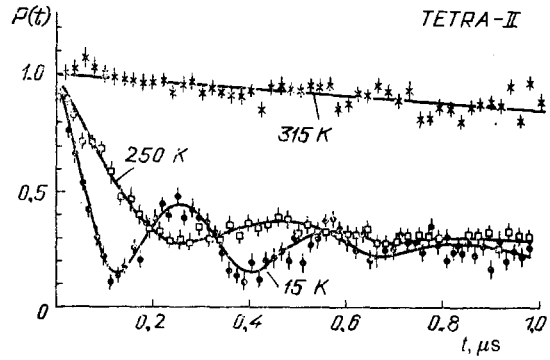

FIG. 17. Oscillations of the polarization of a muon in the tetragonal phase of $YBa_2Cu_3O_7$ (Ref. 75).

$YBa_2Cu_3O_x$ ($x = 6.2$).[74] For $T < 300$ K oscillations were observed in the polarization, with a frequency depending on the temperature and equal to $\nu_\mu = 4$ MHz at $T = 5$ K (Fig. 17). Oscillations in the polarization were observed for 70% of the muons that stopped in the target. The polarization of 30% of the muons was "lost." Subsequently, the experiments were carried out more thoroughly.[75] It was found that no magnetic ordering was observed in the superconducting orthorhombic phase for $T > 2$ K, but in a $YBa_2Cu_3O_{6.4}$ sample ($T_c \approx 60$ K) the depolarization rate increased as the temperature was lowered, which is an indication of an increased magnetic correlation. Those investigators[75] proposed that a spin-glass type of magnetic structure appears.

In the tetragonal form of $YBa_2Cu_3O_{6.2}$ the oscillation frequency decreased with increasing temperature. For $T \geqslant 250$ K the oscillations were not observed (Fig. 18). The frequency observed at $T = 2.4$ K corresponds to a field at the muon of $h_\mu \approx 240$ G. As can be seen, for $T < 40$ K the precession frequency increases slowly as the temperature is lowered. This effect can be explained by an ordering that occurs[5)] at $T = T_{N2}$ in the magnetic moments of the d electrons of copper in the Cu–O chains.[8] The results are in good agreement with the results of neutron diffraction investigations of the magnetic structure of $NdBa_2Cu_3O_x$ (Ref. 76), where for $x = 6.2$, $T_{N2} = 40$ K. The value of T_{N2} falls off as the temperature is increased.

Experiments carried out at $T < T_N$ in a weak field perpendicular to the initial muon polarization showed that for some of the muons the precession frequency corresponds to

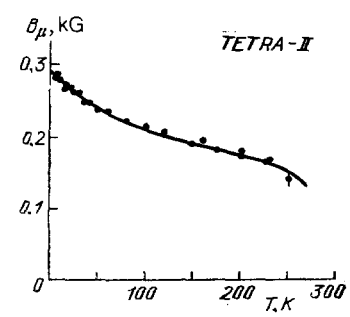

FIG. 18. Temperature dependence of the field at the muon in the tetragonal phase of $YBa_2Cu_3O_x$ (Ref. 75).

the external field.[75] For $T < T_N$ the disordered phase thus exists in the sample. The total polarization of the ensemble of muons can be written as

$$\mathbf{P}(t) = \mathbf{P}_A(t) + \mathbf{P}_P(t), \tag{6.11}$$

where $\mathbf{P}_A$ and $\mathbf{P}_p$ are the fractions corresponding to the muons that have stopped in the ordered (antiferromagnetic) and in the disordered phases. Furthermore, part of the polarization is not observed (is lost). For $T \approx 200$ K, $\mathbf{P}_p$ comprises about 10%, and for $T \leqslant 10$ K, $\mathbf{P}_p = 0$, $\mathbf{P}_A$ comprises $\approx 70\%$, and therefore $\approx 30\%$ of the polarization is lost (Fig. 19). As the temperature is raised, $\mathbf{P}_A$ decreases and $\mathbf{P}_p$ correspondingly, increases. At $T = 300$ K, 100% of the muons are found in the paramagnetic state of the sample.

To explain the nature of the lost polarization, an experiment was performed[75] to recover the polarization in longitudinal fields. It was found that in a field $\mathbf{H}_{ext} \approx 2$ kG the polarization was completely restored and 100% of the polarization of the muons was observed. From this result the investigators concluded that polarization is lost because of a spread $\Delta h \approx 200$ G in the local fields at the muon. Since $\Delta h \approx B$, and the temperature dependence of the lost fraction is the same as for $\mathbf{P}_A$, Nishida *et al.*[75] suggested that the lost polarization is related to muons that are located in the magnetically ordered phase, but in different states such as on some kind of defect (impurities, vacancies, and the like). Quite recently a paper has appeared in which it was reported that in a $YBa_2Cu_3O_6$ sample two frequencies of oscillation of the muon polarization were observed.[77] Here, 80% of the muons were located in a field $h_\mu \approx 300$ G and 20% in a field $h_\mu \approx 1300$ G. This result probably is an indication of the presence of two crystallographically nonequivalent states for the muon. It is possible that the state with $h_\mu \approx 1300$ G is associated with missing oxygen in the Cu–O chain. The fall-off in the depolarization rate for $T > 200$ K indicates diffusion. A study of the polarization in zero field for $T > T_N$ also indicates diffusion at high temperatures. For $T < 200$ K we can assume that the muon does not diffuse. This conclusion is in agreement with μ SR investigations of rare-earth orthoferrites $ReFeO_3$.[71,72]

The transition into the antiferromagnetic state of the orthorhombic ceramic $YBa_2Cu_3O_x$ has been studied[78–80] as a function of the oxygen content, $6.0 < x \leqslant 6.5$. No sharp transition into a magnetically ordered state was observed in the samples. The transition occurred over a range of several tens of degrees, and consequently one can speak only of some

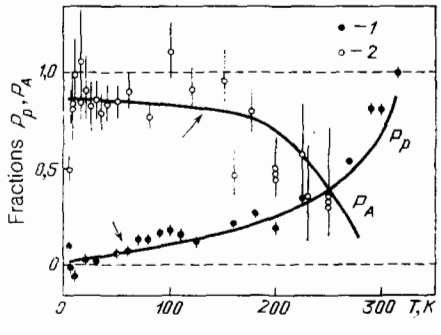

FIG. 19. Temperature dependences of the fractions P_p (*1*) and P_A (*2*).

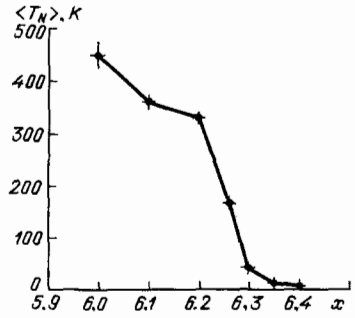

FIG. 20. Dependence of $\langle T_N \rangle$ on the oxygen content in the orthorhombic phase of $YBa_2Cu_3O_x$ (Ref. 78).

average transition temperature $\langle T_N \rangle$. As shown in Fig. 20, the value of $\langle T_N \rangle$ was found to have a strong dependence on the oxygen content. As was the case in Refs. 74 and 75, the polarization precessed at the frequency $\nu_\mu \approx 4$ MHz, which corresponds to a field at the muon of $h_\mu \approx 300$ G. The local field at the muon remains unchanged for $x < 6.25$. For the case of slowly annealed samples and samples with $x = 6.348$ and $x = 6.400$, a sharp superconducting transition was observed, at $T_c = 25$ K and 33 K, respectively. For these same samples, while in the superconducting state, a transition into the antiferromagnetic state was observed, with $\langle T_N \rangle \approx 10$ K and 5 K, respectively. At the same time, a frequency shift was observed.

Precession of the polarization has been observed[81] in zero field for a $YBa_2Cu_3O_x$ sample ($T_c = 90$ K) for $T < 250$ K at a frequency $\nu_\mu \approx 4$ MHz and a small amplitude (about 10% of the total amplitude). However, the sample was not a single phase, and the precessing signal was most likely due to muons that had stopped in the non-superconducting tetragonal phase.

Schneider *et al.*[82] have observed a nonmonotonic temperature dependence of the Knight shift at the muon and of the rate of depolarization at low temperatures for $YBa_2Cu_3O_x$ samples ($T_c = 92$ K). When the temperature was lowered a nonprecessing component appeared ($\approx 18\%$ at $T \approx 9$ K), whereas, at $T \approx 85$ K all the muons precessed. A similar picture was observed in Ref. 80 for samples with $6.38 \leqslant x \leqslant 6.48$, where, as the investigators point out, the superconducting and the magnetically ordered states coexist: at $T \approx 70$ K the Knight shift has a minimum, and for $T \leqslant 10$ K the component rapidly decays. It is possible that this behavior of the polarization is related to the establishment of a spin-glass type of magnetic ordering. These results agree with the results of Ref. 75, where in a superconducting sample at $T < 7$ K ($T_c = 60$ K, $x = 6.4$), rapid relaxation of the component was observed ($t \approx 300$ ns). However, Weidinger *et al.*,[83] have stated that in a superconducting sample of $YBa_2Cu_3O_x$ ($T = 90$ K) no rapid relaxation of the muon spin was found down to $T = 35$ mK, and therefore, the spin-glass type of magnetic ordering was not observed.

Investigations of superconducting samples of $YBa_2(Cu_{1-y}Fe_y)_3O_7$ worthy of notice are those reported in Refs. 84–86, where a nonmonotonic temperature dependence of the depolarization rate for $T < T_c$ was observed. In samples with $y = 0.08$ at $T \approx 15$ K a minimum was observed

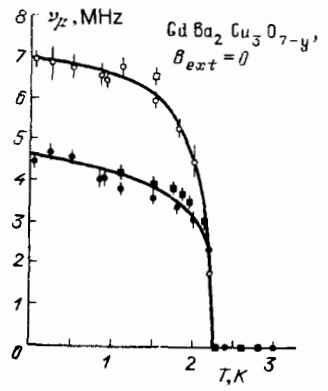

FIG. 21. Temperature dependence of the precession frequencies in a superconducting sample of $GdBa_2Cu_3O_x$ (Ref. 87).

in the depolarization rate, indicative of the freezing-in of the magnetic moments of the Cu. Mössbauer spectra of ^{57}Fe were also measured by Saitovich *et al.*,[85] who showed that the Fe ions are located in three different sites in the lattice. The authors[85] believe that the results indicate the existence of antiferromagnetic ordering, but this has not been borne out by data from μ SR experiments performed in the same work.[85]

It is well known that when yttrium is replaced by the rare-earth ions Gd, Dy, Ho, or Er, the superconducting properties of the ceramic are unchanged, but in these systems, unlike $YBa_2Cu_3O_x$, antiferromagnetic ordering is distinctly seen in the magnetic moments of the rare-earth metal ions in the orthorhombic (superconducting) phase at the temperature T_{N3} (Table II; Ref. 8). Also of note is the complete absence of any regular relation between T_{N3} and the value of the magnetic moments of the Re ions.

Precession at a frequency ≈ 4.6 MHz has been observed[81,87-90] in the polarization of the muon spin in samples of $GdBa_2Cu_3O_x$ (the field at the muon is 340 G), while Ref. 87 reports the observation of two frequencies at $T<2.3$ K (Fig. 21). The higher frequency (≈ 7 MHz) corresponds to a field at the muon of $h_\mu \approx 520$ G. The frequencies do not depend on T_c, and the ratio of the amplitudes does not change. For the sample with $T_c = 60$ K the ratio of the amplitudes is $A_{4.6}/A_7 \approx 2.5$, and for the sample with $T_c = 90$ K, the ratio is $A_{4.6}/A_7 \approx 5$. It is possible that the higher frequency is due to the presence of the tetragonal phase.[6)] However, for a sample with $T_c = 90$ K, Golnik *et al.*,[81] have observed precession only at a single frequency ≈ 4 MHz for $T<300$, with an amplitude corresponding to 50% of the muons stopping within the target (Fig. 22). This result is similar to that obtained in the same investigation for the behavior of the muon polarization in a polyphase sample of $YBa_2Cu_3O_x$ ($T = 90$ K). As Fig. 22 shows, for $T<20$ K the precession frequency falls off simultaneously with a rapid increase in the relaxation rate. The temperature dependence of the relaxation rate of the precessing component is similar to that of $\lambda(T)$ observed in Ref. 87, for nonprecessing polarization for $T>T_N$ (Fig. 23). We note that in this investigation a considerable fraction of the polarization was not observed (the initial asymmetry coefficient was about 0.15, which corresponds to less than two thirds of the total polarization).

A single precession frequency, corresponding to the lower frequency reported in Ref. 87 was also observed[90] at $T \approx 2$ K in a sample of $CdBa_2Cu_3O_x$ ($T_c = 90$ K). The amplitude of the precessing signal was, however, not provided.

The superconducting sample $ErBa_2Cu_3O_x$ has been studied at $T \geqslant 4.2$ K in the work reported in Ref. 91. Magnetic ordering was not seen, and the depolarization rate remained unchanged ($\Lambda \approx 0.2\ \mu s^{-1}$) for 4.6 K $< T <$ 270 K. As is shown in Table II, $T_{N3} = 0.5$ K for systems with Er. The experiment of Ref. 91 showed that for $T \approx 4$ K the fluctuations of the magnetic moments of the *f*-shells of the Er ions are small.

In non-superconducting samples of $ErBa_2Cu_3O_x$ for $x = 6.11$, 6.34, and 6.40 the values obtained for T_N are 300 K, 250 K, and 20 K, respectively.[92] For $T<10$ K the precession frequency ν_μ increases and becomes higher than in $YBa_2Cu_3O_x$ (i.e., $T_{N3} \lesssim 10$ K). Maletta *et al.*[92] found the value $T_{N3} \approx 0.5$ K, which agrees with the results of neutron diffraction experiments (see Table II).

In the orthorhombic phase of $HoBa_2Cu_3O_x$ magnetic ordering was not seen for $T>3$ K.[90,91,93-96] In the first experiments[90,91,93,94] an abrupt increase was observed in the fluctuations for $T<5$ K, and, short-range order was established at $T \approx 2$ K. No precession frequency in zero field was observed.[7)] On the other hand, precession was observed[95] in the polarization of the muon spin in zero external field at a temperature $T<300$ mK. Detailed experiments were carried out in the temperature range 39 mK $< T <$ 50 K in the work reported in Ref. 96. It was found that the polarization could be well described by the formula

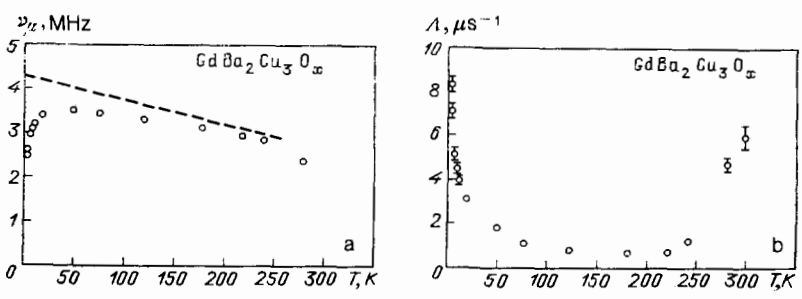

FIG. 22. Temperature dependences of the precession frequency and of the depolarization rate in superconducting $GdBa_2Cu_3O_x$ with $T_c = 90$ K (Ref. 81).

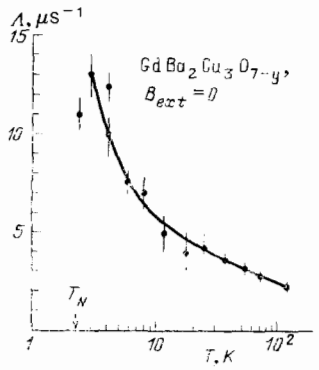

FIG. 23. Temperature dependence of the depolarization rate in superconducting $GdBa_2Cu_3O_x$ ($T_c = 60$ K) for $T > T_N$ ($B = 0$) (Ref. 87).

$$P(t) = A_{\parallel} e^{-\lambda t} + A_{\perp} e^{-\sigma^2 t^2} \cos(\mu_\mu t), \qquad (6.12)$$

where $A_{\parallel} + A_{\perp} = 1$. Thus, 100% of the polarization was measured. The temperature dependences of the asymmetry coefficients $A_{\parallel}$ and $A_{\perp}$ are shown in Fig. 24.

The oscillating component is weak at $T = 2.4$ K and completely unobservable at $T = 5$ K. However, even at $T = 39$ K the pronounced oscillations are rapidly damped. This means that the fluctuations in the magnetic field are of the same order of magnitude as the average value of the field. Figure 25 shows the temperature dependence of the oscillating frequency. For $T < 75$ mK, the frequency is $\nu_\mu \approx 2.5$ MHz (which corresponds to a field $h_\mu \approx 185$ G at the muon), and the frequency falls off rapidly in the range 75 mK $< T <$ 150 mK to 1.5 MHz (the field at the muon is $h_\mu \approx 111$ G). As the temperature is raised further ($T \gtrsim 0.6$ K) the frequency decreases again, and goes to zero at $T = 5$–6 K. Figure 24 shows the value of $A_\perp \neq 0$ up to $T = 50$ K, but a Gaussian form of relaxation after ω_μ goes to zero gives a poor description of the observed picture. In the temperature range where $\omega_\mu \neq 0$ the second moment σ is independent of the temperature and corresponds to fluctuations of the field of $\langle \Delta h_l^2 \rangle^{1/2} \approx 82$ G along the average direction. The variation of the frequency is accounted for by the reorientation of the magnetic moments of Ho from along the c axis for $T < 100$ mK to parallel to the a axis for $T > 100$ mK.[96]

The exponential relaxation varies nonmonotonically: for $T \approx 4.5$ K there is a sharp peak in the relaxation rate of λ, which is in agreement with the results of Refs. 90 and 94. For $T > 5$ K the temperature dependence $\lambda(t)$ is well described by an Arrhenius plot, with an activation energy $U \approx 15$ K.[96]

A series of experiments have been recently reported for $Pr_yY_{1-y}Ba_2Cu_3O_x$.[77,97,98] For samples with $x = 7.0$ and $y = 1.0$, 0.8, 0.6, and 0.54, the Neél temperatures obtained were $T_N = 275$, 220, 35, and 20 K, respectively.[98] The local field at the muon depends on the temperature: for $y = 1.0$ it decreases for $T < 17$ K. It was concluded by Cooke *et al.*[98] that this result is due to the ordering of the magnetic moments of Cu in the chain ($T_{N2} \approx 17$ K). Ordering of the magnetic moments of the Pr has been observed[97] at $T < 5$ K (see Table II). For $y \approx 0.5$ magnetic ordering and superconductivity coexist.[98] Two frequencies have been observed[77] in $PrBa_2Cu_3O_6$: $\nu_1 \approx 3.1$ MHz ($h_\mu \approx 230$ G, 10% of the muons) and $\nu_1 \approx 1.0$ MHz ($h_\mu \approx 75$ G, 90% of the muons). For $T < 150$ K the relaxation rate increased, and for $T < 100$ K it was not possible to obtain any information.

Experiments that have been carried out with $YBa_2Cu_3O_xH_y$ are interesting.[99] For $x = 7.0$ oscillations were observed for $y > 0.5$. It should be noted that in superconducting samples the depolarization rate goes as $\Lambda \sim y^{-1}$.

Thus, all ceramic superconductors exhibit magnetic ordering corresponding to $T_N \ll T_c$. In the transition into the antiferromagnetic state the relaxation rate for $T > T_N$ does not have the critical character that is characteristic of second order phase transitions in ordinary materials. The low oscillation frequencies in the antiferromagnetic phase imply that the muons in the lattice are relatively distant from the rare earth ions. As has been noted previously, the muons do not diffuse in orthoferrites (having the orthorhombic structure) at $T < 100$ K, and do form muon-oxygen bonds with the oxygen. One might anticipate a similar behavior of the muon in superconducting ceramics of the type $ReBa_2Cu_3O_x$. A detailed analysis of the dipole fields at the muon has been made[96] for various states of the undistorted lattice. Birrer *et al.*[96] have concluded that the measured values of the local field at the muon are also in good agreement with the calculated values for a muon that is located at a distance ≈ 1 Å from the oxygen in the Cu–O chain (coordinates $0.171a$, $0.5b$, $0.065c$), i.e., a muon–oxygen bond is formed. In nonsuperconducting samples some of the oxygen is missing from the Cu–O chains; therefore it is favorable for the muon to

TABLE II. Magnetic ordering temperature T_{N3} and atomic magnetic moments of the rare-earth sublattice of $ReBa_2Cu_3O_x$ (Ref. 8).

Re	Y	Nd	Er	Dy	Gd	Pr
T_{N3}, K	0.35	0.5	0.5	1.0	2.2	17
μ, Units of μ_B			4.9	7.2	7.4	0.24

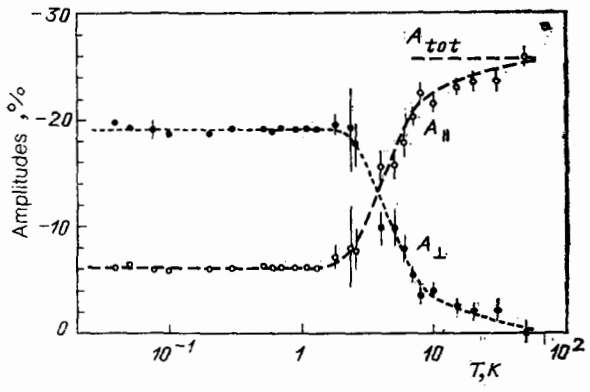

FIG. 24. Temperature dependences of the parameters $A_{\perp}$ and $A_{\parallel}$ in superconducting $HoBa_2Cu_3O_x$ (Ref. 95).

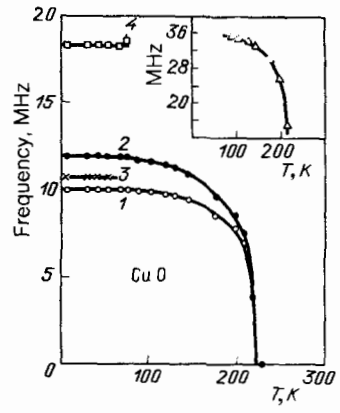

FIG. 26. Precession frequencies in CuO (Ref. 100).

occupy another site in the lattice.[8)] In particular, for the tetragonal phase of $ReBa_2Cu_3O_6$ there are no oxygen ions in the plane $z = 0$, and the muon can occupy the site between two oxygen ions ($0.0a$, $0.5b$, $0.159c$). A calculation of the dipole field at the muon in this site for the case of a nondistorted lattice[96] is in good agreement with the experimental measurements of the field in the tetragonal phase of $YBa_2Cu_3O_x$.

Also interesting is the investigation of antiferromagnetic ordering in the components used in preparing superconducting ceramics: $BaCuO_2$, BaY_2CuO_5, and CuO.[101,102] In $BaCuO_2$ crystals a single precession frequency is observed for $T < T_N = 11$ K., which follows from the Brillouin function for angular momentum $J = 0.5$, while in the low temperature limit somewhat below 14 MHz ($B \approx 1$ kG).

For a sample of BaY_2CuO_5 five precession frequencies have been observed for temperatures $T < T_N = 15.3$ K. The lowest frequency was about 3 MHz, and the highest was about 9 MHz. These frequencies correspond to five different positions of the muon in the lattice, which do not change in this temperature range.

The highest ordering temperature, $T_N = 226$ K, was found for CuO. At temperatures $T < 60$ K four frequencies were readily identified (Fig. 26), and of them, two frequencies, 10 and 12 MHz have equal amplitudes ($\approx 3\%$), and their temperature dependences are governed by the Brillouin curve, while the other two frequencies (11 MHz and 18 MHz) also have equal amplitudes ($\approx 6\%$), but the lower frequency is observed for $T < 60$ K, and the higher is observed at $T < 90$ K. For $T > 100$ K a third frequency appears in place of these two, at 35 MHz with an intensity that increases with temperature, and for $T \approx 220$ K it corresponds to 30% of the muons that have come to rest in the target. The authors of Ref. 101 suggest that the appearance of the new frequency at 35 MHz is due to the localization of the muons near the Cu^{2+} ion, which is in a triplet state.

Experiments with lanthanum ceramics have been focused mainly on comparing the nature of the antiferromagnetism in La_2CuO_{4-y} with that of $La_{2-x}Sr_xCuO_4$. A deficiency of divalent oxygen (O^{2-}) and the replacement of trivalent lanthanum (La^{3+}) by divalent strontium (Sr^{2+}) creates holes that suppress the antiferromagnetic ordering. The magnetic properties of La_2CuO_{4-y} are very sensitive to a change in the oxygen content in a narrow range $0 < y < 0.03$: $T_N \approx 290$ K for $y = 0.03$ and $T_N \approx 0$ for $y = 0$. Results of experiments in zero field with polycrystalline single-phase samples with various concentrations of oxygen[103] are shown in Fig. 27. It can be seen that T_N varies from 15 K to 300 K, and the precession frequency as $T \to 0$ depends only weakly on y. For example, for $T_N \approx 295$ K, $\nu_\mu \approx 5.8$ MHz ($h_\mu \approx 429$ G) and for $T_N \approx 10$ K, $\nu_\mu \approx 5.1$ MHz ($h_\mu \approx 377$ G).[104] As T_N is approached the relaxation rate of the precessing component increases sharply.[105] Unfortunately, we know of no μ SR experiments with samples having a large oxygen deficit, in particular values of y where the transition to the superconducting state is observed.[9)]

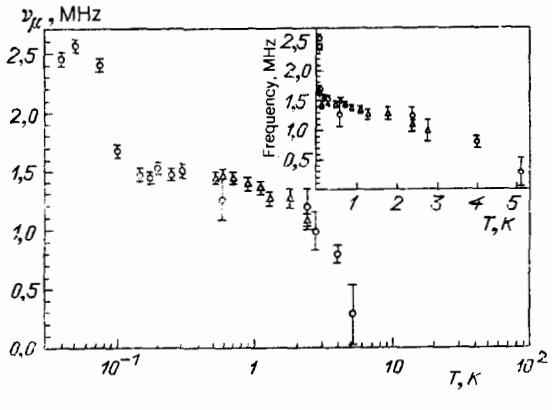

FIG. 25. Temperature dependence of the oscillation frequency of the polarization in $HoBa_2Cu_3O_x$ (Ref. 95).

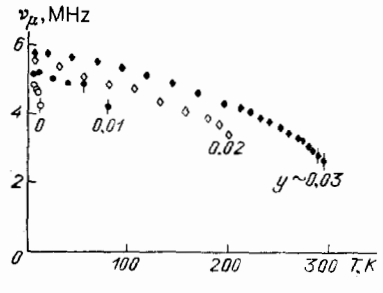

FIG. 27. Temperature dependence of the precession frequency of the polarization in non-superconducting La_2CuO_{4-y} ceramics for various values of y (Ref. 103).

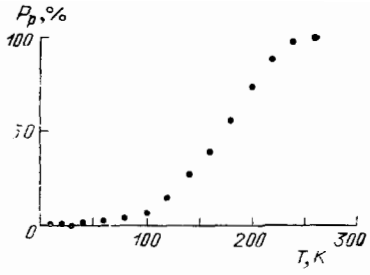

FIG. 28. Temperature dependence of the amplitude of the precessing component in a weak external field $B = 100$ G in a single crystal of La_2CuO_{4-y} (Ref. 103).

In all the investigations, precession has been observed for 50–60% of the muons that have stopped in the target. It has been shown[104] in experiments in a transverse field $B = 500$ G that 30 to 40% of the muons are found in positions where the local field is $h_\mu \leqslant 10$ G. Uemura *et al.*,[104] were not able to determine whether this fraction is associated with muons located in macroscopic disordered regions or with muons located in interstitial sites, where the local field is zero. Experiments[103] with a single crystal of La_2CuO_{4-y} in a transverse field $B = 100$ G show that magnetic ordering occurs gradually, and at low temperatures the paramagnetic fraction is completely absent (Fig. 28). The possible presence of a paramagnetic fraction has been related to the polycrystalline nature of the samples.[104,105]

In samples of $La_{2-x}Sr_xCuO_4$ the temperature of magnetic ordering depends strongly on the Sr content[83,107,108] (as is well known, the superconducting transition occurs for $x \geqslant 0.07$)[10)] For $T < T_N$ a rapidly attenuating fraction was observed in addition to the oscillating component.[108] For $x < 0.05$ the oscillation frequency at low temperatures corresponds to that observed in La_2CuO_{4-x} samples ($y = 0$–0.03), but even for $x = 0.05$, $\nu_\mu = 4.1$ MHz ($h_\mu \approx 303$ MHz) (Fig. 29).[108] The rate of depolarization of the oscillating component increases sharply as T_N is approached. In the paramagnetic region as the temperature approaches T_N there is an increase in the depolarization rate, associated with dynamic fluctuations in the magnetization (Fig. 30).[108]

In the first experiments with $x \geqslant 0.1$, magnetic ordering was not observed. However, measurements of the specific heat in a superconducting sample of $La_{1.85}Sr_{0.15}CuO_{4-y}$

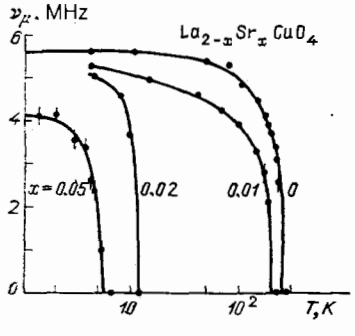

FIG. 29. Temperature dependence of the oscillation frequency of the polarization in non-superconducting samples of $La_{2-x}Sr_xCuO_4$ for various values of x (Ref. 106).

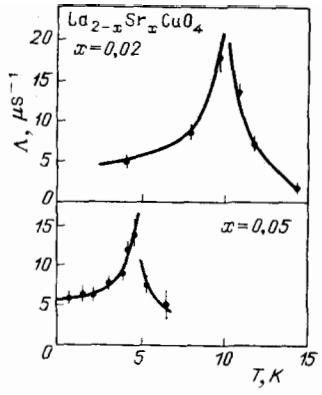

FIG. 30. Depolarization rate in non-superconducting $La_{2-x}Sr_xCuO_4$ for $T \approx T_N$ (Ref. 106).

have shown that for $t < 0.3$ K magnetic ordering occurs.[109] Magnetic ordering of the ^{139}La nuclei has been detected by nuclear quadrupole resonance in superconducting samples of $La_{2-x}Ba_xCuO_4$.[110] It was shown that superconductivity and magnetic ordering are competing mechanisms. For $x = 0.05$ the superconducting transition temperature is $T_c = 6$ K and $T_N = 2$ K, but already at $x = 0.08$, $T_c = 28$ K and $T_N < 1.3$ K. We are not aware of any μ SR experiments with samples of $La_{2-x}Ba_xCuO_4$, but a recent paper[83] has reported magnetic ordering of $La_{2-x}Sr_xCuO_4$ for $x \leqslant 0.07$.[11)] For samples with $x = 0.07$ ($T_c = 14$ K) a rapid relaxation has been observed at $T = 35$ mK for oscillations with a frequency $\nu \approx 1.5$ MHz ($h_\mu \approx 111$ kG), but at $T = 2.2$ K, only a rapid depolarization was observed. Bezhitadze *et al.*,[91] have inferred the establishment of a spin-glass type of magnetic structure with field cooling for a superconducting sample with $x = 0.07$ at $T_1 \approx 10$ K from the increase in the depolarization rate and the decrease in the asymmetry coefficient for the precessing component. In samples with $x = 0.10$ ($T_c = 26$ K) and $x = 0.15$ ($T_c = 32$ K) the oscillations were not observed even at $T = 35$ mK, but depolarization was observed: the asymmetry first decreased by a factor of e in 2.3 and 1 μs, respectively. The depolarization rate for $T < 1$ K was essentially independent of the temperature and fell abruptly for $T > 2$ K.[83]

These results are supported by more recent experiments with single crystals of $La_{1.88}Sr_{0.12}CuO_4$ (Ref. 111), which go over into the superconducting state at $T_c = 35$ K. The μ SR signal varies rapidly for $T < 20$ K, and for $T \lesssim 8$ K corresponds to the onset of magnetic ordering. Torikai *et al.*,[111] suggest that the magnetic structure corresponds to a spin glass.

To conclude we shall discuss briefly investigations of samples related to the high-T_c superconductors $Bi_2Sr_2CaCu_2O_x$ and $Bi_2Sr_2CaCu_3O_x$. Partial replacement of Sr or Ca by yttrium while the stoichiometry is maintained removes the superconductivity, but brings about magnetic ordering.[112,113]

The transition into the magnetically ordered state was observed[112] for a polycrystalline sample of $Bi_2Sr_2YCu_2O_{8.5}$ at $T \approx 295$ K. In addition to the signal oscillating at the frequency $\nu \approx 0.4$ MHz ($h \approx 30$ G), a component was observed that did not oscillate. The depolarization of the oscillating component was governed by inhomogeneous broadening. In

a transverse field $B = 220$ G two nearly equal frequencies of about the same intensity but with different widths were observed for $T > 200$ K. For $T < 200$ K the amplitude of the narrower line was reduced by a factor of 1/3, presumably because of the diffusion of the muon. Yang *et al.*,[113] also studied polycrystalline samples of $Bi_2Sr_2YCu_2O_x$, but, unlike the work reported in Ref. 112, four frequencies were observed at $T = 3.7$ K, of which three frequencies, 0.49, 3.67, and 4.47 MHz were dominant, and the frequency of 12 MHz rapidly relaxed ($\lambda \sim 10^7\ s^{-1}$). In addition to the oscillating components, a paramagnetic fraction was also observed. As in the previous investigations, the transition into the magnetically ordered state is not sharp, so that one can speak only of an average temperature $\langle T_N \rangle \approx 210$ K. As we see, for the sample of Ref. 113, this is lower than for the sample of Ref. 112. The frequency 0.49 MHz (Ref. 113) can be identified with the 0.4 MHz of Ref. 112, since the lattice constant for the sample of Ref. 112 was larger.

In the polycrystalline sample of $Bi_2Sr_2YCaCu_2O_x$ oscillations in the polarization were not observed, but at $T \approx 15$ K a spin-glass state was established.[113]

Muon spin rotation experiments thus show that all high-T_c superconductors are characterized by a magnetically ordered state, as a rule, for $T \ll T_c$. However, the experiments with ceramics do not always have an unambiguous interpretation. For a good interpretation the μ SR experiments require work with single crystals. In this connection we note that in a so-far unique experiment with a single crystal of La_2CuO_{4-y}, 100% polarization was observed[103] and there was no "lost" fraction. We also note that by the technology of the preparation of high-T_c superconductors based on Bi and Ta one can prepare large single crystals that are suitable for studies by the muon spin rotation method. Investigations of magnetic ordering in these structures would be highly desirable.

[1)] Crystallographically equivalent voids may be nonequivalent in a magnetic sense. For example, in a single crystal of Fe magnetized along the [111] direction the internal magnetic field in the octahedra (the centers of the faces of the unit cells) takes on two different values (see, e.g., Ref. 3).

[2)] The sample is assumed to be untextured.

[3)] For non-superconducting samples we neglect the paramagnetic and diamagnetic susceptibilities $\chi \approx 10^{-5}$–10^{-6}. Consequently $B = H_{ext}$.

[4)] We have discarded the terms of higher order in h_0/B.

[5)] In $ReBa_2Cu_3O_x$ compounds the three antiferromagnetic ordering temperatures are different:[8] T_N refers to the ordering of the magnetic moments in the Cu–O plane, T_{N2} to the Cu–O chains, and T_{N3} is defined by the ordering of the magnetic moments of the rare-earth elements.

[6)] In Ref. 89 two frequencies were also observed for the tetragonal phase of Y-Ba-Cu-O for $T < 240$ K: one known previously and one somewhat higher (≈ 4.3 MHz). The sum of the amplitudes of the polarizations precessing at the two frequencies corresponded to 40% of the muons that have stopped in the target.

[7)] In the tetragonal phase in $HoBa_2Cu_3O_x$ at $T < 260$ K precession at a frequency of ≈ 4 MHz was observed. With a decrease in the temperature, for $T < 5$ K a rapid increase in the rate of depolarization was observed, indicating the freezing-in of the magnetic moments of Ho.[90,94]

[8)] The observation of several closely spaced precession frequencies, corresponding to different values of the Knight shift at the muon, in the superconducting ceramics $HoBa_2Cu_3O_x$ and $ErBa_2Cu_3O_x$ in the temperature range $50 < T < 300$ K shows that the muon can be localized in different sites.[100]

[9)] As is known, the superconducting transition in $LaO(LaCuO_3)$ systems occurs at $T \approx 30$–40 K (see e.g., Ref. 106).

[10)] Ordinarily, the oxygen content is not monitored, and therefore we must refer to the samples as $La_{2-x}SrCuO_{4-y}$.

[11)] Single-phase samples were studied.

[1] V. P. Smilga, *Muons in Matter* [in Russian], Joint Institute for Nuclear Research, Dubna, 1976.
[2] V. P. Smilga, Summer School Lectures [in Russian], Engineering Physics Institute, Moscow (1976).
[3] Yu. M. Belousov, V. N. Gorelkin, A. L. Mikaélyan, V. Yu. Miloserdin, and V. P. Smilga, Usp. Fiz. Nauk **129**, 3 (1979) [Sov. Phys. Usp. **22**, 679 (1979)].
[4] D. Saint James, G. Sarma, and E. J. Thomas, Type II Superconductivity, Pergamon Press, Oxford (1969).
[5] I. G. Ivanter and V. P. Smilga, Zh. Eksp. Teor. Fiz. **55**, 548 (1968) [Sov. Phys. JETP **28**, 286 (1969)].
[6] L. P. Gor'kov and N. V. Kopnin, Usp. Fiz. Nauk **156**, 117 (1988) [Sov. Phys. Usp. 850 (1988)].
[7] L. N. Bulaevskii, V. L. Ginzburg, and A. A. Sobyanin, Zh. Eksp. Teor. Fiz. **94**(7), 355 (1988) [Sov. Phys. JETP **67**, 1499 (1988)].
[8] Yu. A. Izyumov, N. M. Plakida, and Yu. N. Skryabin, Usp. Fiz. Nauk **159**, 621 (1989) [Sov. Phys. Usp. **32**, 1060 (1989)].
[9] Yu. V. Kopaev, Usp. Fiz. Nauk **159**, 567 (1989) [Sov. Phys. Usp. **32**, 1033 (1989)].
[10] A. A. Abrikosov, *Fundamentals of the Theory of Metals* [in Russian], Nauka, M., 1987.
[11] L. P. Gor'kov, Zh. Eksp. Teor. Fiz. **36**, 1918 (1959) [Sov. Phys. JETP **9**, 1364 (1959)]; Zh. Eksp. Teor. Fiz. **37**, 1407 (1959) [Sov. Phys. JETP **10**, 998 (1960)].
[12] G. Eilenberger, Phys. Rev. **153**, 584 (1967).
[13] A. A. Abrikosov, Zh. Eksp. Teor. Fiz. **32**, 1442 (1957) [Sov. Phys. JETP **5**, 1174, 1957)].
[14] G. Lasher, Phys. Rev. **140A**, 523 (1965).
[15] S. A. Gordyunin, V. P. Smilga, and V. I. Fesenko, Pis'ma Zh. Eksp. Teor. Fiz. **47**, 34 (1988) [JETP Lett. **47**, 40 (1988)].
[16] A. D. Sidorenko and V. P. Smilga, Sverkhprovodimost' (KIAE) **2**(4) 98 (1989).
[17] G. M. Fikhtengol'ts, *Course in Differential and Integral Calculus* [in Russian], Vol. III, Gostekhizdat, Moscow, Leningrad (1949).
[18] E. T. Whittaker and G. N. Watson, *A Course in Modern Analysis*, Fourth Ed. Cambridge University Press (1940). [Russ. transl., Fizmatgiz, M., 1963].
[19] V. M. Samoilov, Sverkhprovodimost' (KIAÉ) **2**(9), 56 (1989).
[20] V. L. Ginzburg, Zh. Eksp. Teor. Fiz. **23**, 236 (1952).
[21] A. V. Balatskiĭ, L. I. Burlachkov, and L. P. Gor'kov, Zh. Eksp. Teor. Fiz. **90**, 1478 (1986) [Sov. Phys. JETP **63**, 866 (1986)].
[22] A. D. Sidorenko, V. P. Smilga, and V. I. Fesenko, Sverkhprovodimost' (KIAÉ) **2**(8), 17 (1989).
[23] L. J. Campbell, M. M. Doria, and V. G. Kogan, Phys. Rev. B **38**, 2439 (1988).
[24] D. R. Harshman, L. F. Schneemeyer, J. N. Waszczak *et al.*, Phys. Rev. B **39**, 851 (1989).
[25] F. I. Larkin and Yu. N. Ovchinnikov, J. Low Temp. Phys. **34**, 409 (1979).
[26] E. H. Brandt, J. Low Temp. Phys. **28**, 263 (1977); **28**, 291 (1977).
[27] E. H. Brandt, Phys. Rev. B **34**, 6514 (1986).
[28] R. Schmucker and E. H. Brandt, Phys. Stat. Solidi B **79**, 479 (1977).
[29] E. H. Brandt and U. Essman, Phys. Stat. Solidi B **144**, 13 (1987).
[30] E. H. Brandt, J. Low Temp. Phys. **64**, 375 (1986).
[31] E. H. Brandt, Physica C **162-164**, 257 (1989).
[32] A. Seeger, Phys. Lett. A **77**, 259 (1979).
[33] E. H. Brandt and A. Seeger, Adv. Phys. **35**, 189 (1986).
[34] D. R. Nelson, Phys. Rev. Lett. **60**, 1973 (1988).
[35] E. H. Brandt, Phys. Rev. Lett. **63**, 1106 (1989).
[36] R. Wördenweber and P. H. Kes, Phys. Rev. B **34**, 494 (1986).
[37] R. Meier-Hirmer, H. Kupfer, and H. Scheurer, Phys. Rev. B **31**, 183 (1985).
[38] E. H. Brandt, Phys. Rev. Lett. **50**, 1599 (1983).
[39] A. Isihara, Statistical Physics, Academic Press, N.Y., 1971 [Russ. transl., Mir, M., 1973].
[40] E. M. Lifshitz and L. P. Pitaevskii, Statistical Physics, Pergamon Press, N.Y., 1980 [Russ. original, Nauka, M., Part II, 1978].
[41] P. G. de Gennes, Superconductivity of Metals and Alloys, Benjamin, N.Y., 1966.
[42] P. Zimmerman, H. Keller, W. Kundig *et al.* (in press).
[43] E. H. Brandt, Phys. Rev. B **37**, 2349 (1988).
[44] E. H. Brandt, Phys. Stat. Solidi B **51**, 345 (1972).
[45] B. Pümpin, H. Keller, W. Kundig *et al.*, Phys. Rev. B **42**, 8019 (1990).

[46]W. Barford and J. M. F. Gunn, Physica C **156**, 515 (1988).
[47]S. G. Barsov, A. A. Vasil'ev, A. L. Getalov *et al.*, Sverkhprovodimost' (KIAÉ) **2**(5), 42 (1989).
[48]B. Pümpin, H. Keller, W. Kundig *et al.*, Physica C **153-155**, 71 (1988).
[49]G. Aeppli, R. G. Cava, E. J. Ansaldo *et al.*, Phys. Rev. B **35**, 7129 (1987).
[50]W. J. Kossler, J. R. Kempton, X. H. Yu *et al.*, Phys. Rev. B **35**, 7133 (1987).
[51]F. N. Gygax, B. Hitti, E. Lippelt *et al.*, Europhys. Lett. **4**, 473 (1987).
[52]R. Wäppling, O. Hartman, J. P. Senateur *et al.*, Phys. Lett. A **122**, 209 (1987).
[53]D. R. Harshman, G. Aeppli, E. J. Ansaldo *et al.*, Phys. Rev. B **36**, 2386 (1987).
[54]M. Celio, T. M. Riseman, R. F. Kiefl, and J. H. Brewer, Physica C **153-155**, 753 (1988).
[55]A. Schenk, Physica C **153-155**, 1127 (1988).
[56]S. Barth, P. Birrer, D. Cattani *et al.*, Physica C **153-155**, 755 (1988).
[57]P. Birrer, F. N. Gygax, B. Hitti *et al.*, Physica C **153-155**, 765 (1988).
[58]T. M. Riseman, J. H. Brewer, B. R. Cyca *et al.*, Physica C **162-164**, 1555 (1989).
[59]Y. J. Uemura, G. M. Luke *et al.*, Phys. Rev. Lett. **62**, 2317 (1989).
[60]Y. J. Uemura, L. P. Le, G. M. Luke *et al.*, Proc. of the Fifth International Conference on μ SR–Oxford (1990), p. 44, will be published in Hyperfine Interactions **63–65** (1990).
[61]V. G. Grebinnik, V. Duginov, V. A. Zhukov *et al.*, Proc. of the Fifth International Conference on μ SR–Oxford (1990), p. 43, will be published in Hyperfine Interactions **63–65** (1990).
[62]P. Birrer, D. Cattani, J. Cors *et al.*, Proc. of the Fifth International Conference on μ SR–Oxford (1990), p. 41, will be published in Hyperfine Interactions **63–65** (1990).
[63]V. Weber, P. Birrer, F. N. Gygax *et al.*, Proc. of the Fifth International Conference on μ SR–Oxford (1990), p. 40, will be published in Hyperfine Interactions **63–65** (1990).
[64]B. Pümpin, H. Keller, W. Kundig *et al.*, Proc. of the Fifth International Conference on μ SR–Oxford (1990), p. 26, will be published in Hyperfine Interactions **63–65** (1990).
[65]S. G. Barsov, A. L. Getalov, V. P. Koptev *et al.*, Proc. of the Fifth International Conference on μ SR–Oxford (1990), p. 31, will be published in Hyperfine Interactions **63–65** (1990).
[66]R. L. Lichti, T. R. Adams, D. W. Cooke *et al.*, Proc. of the Fifth International Conference on μ SR–Oxford (1990), p. 33, will be published in Hyperfine Interactions **63–65** (1990).
[67]E. M. Forgan, S. L. Lee, S. Sutton *et al.*, Proc. of the Fifth International Conference on μ SR–Oxford (1990), p. 29, will be published in Hyperfine Interactions **63–65** (1990).
[68]E. W. Cooke, R. L. Hutson, R. W. Kwok *et al.*, Phys. Rev. B **37**, 9401 (1987).
[69]P. Birrer, F. N. Gygax, B. Hettich *et al.*, Physica C **158**, 230 (1989).
[70]C. Boekema, Hyp. Int. **17–19**, 305 (1984).
[71]E. Holzshur, W. Kundig, and A. B. Denison, Hyp. Int. **17–19**, 345 (1984).
[72]P. K. Lin, L. Lichti, C. Boekema, and A. B. Denison, Hyp. Int. **31**, 475 (1986).
[73]G. A. Sawatzky and F. Van Der Woude, J. Phys. C **6**, 47 (1974).
[74]N. Nishida, H. Miyatake, D. Shimada *et al.*, Jpn. J. Appl. Phys. **26**, L1856 (1987).
[75]N. Nishida, H. Miyatake, D. Shimada *et al.*, J. Phys. Soc. Jpn. **57**, 597 (1988).
[76]J. W. Lynn, W. H. Li, H. A. Mook, B. C. Scales, and Z. Fisk, Phys. Rev. Lett. **60**, 2781 (1988).
[77]T. M. Riseman, J. H. Brewer, P. M. Grant *et al.*, Proc. of the Fifth International Conference on μ SR–Oxford (1990), p. 62, will be published in Hyperfine Interactions **63–65** (1990).
[78]G. M. Luke, R. F. Kiefl, J. H. Brewer *et al.*, Physica C **153-155**, 759 (1988).
[79]J. H. Brewer, E. J. Ansaldo, J. F. Carolan *et al.*, Phys. Rev. Lett. **60**, 1073 (1988).
[80]J. H. Brewer, J. F. Carolan, W. H. Hardy *et al.*, Physica C **162-164**, 33 (1989).
[81]A. Golnik, J. I. Budnik, B. Chamberland *et al.*, Physica C **153-155**, 166 (1988).
[82]J. W. Schneider, Hp. Baumeller, H. Keller *et al.*, Phys. Lett. A **124**, 107 (1987).
[83]A. Weidinger, Ch. Niedermayer, A. Golnik *et al.*, Phys. Rev. Lett. **62**, 102 (1989).
[84]W. J. Kossler, X. H. Yu, A. Greer *et al.*, Proc. of the Fifth International Conference on μ SR–Oxford (1990), p. 48, will be published in Hyperfine Interactions **63–65** (1990).
[85]E. B. Saitovitch, F. J. Litterst, K. Nagamine *et al.*, Proc. of the Fifth International Conference on μ SR–Oxford (1990), p. 59, will be published in Hyperfine Interactions **63–65** (1990).
[86]S. Okuma, H. Miyatake, N. Nishida *et al.*, Proc. of the Fifth International Conference on μ SR–Oxford (1990), p. 69, will be published in Hyperfine Interactions **63–65** (1990).
[87]A. Golnik, Ch. Niedermayer, E. Recknagel *et al.*, Phys. Lett. A **125**, 71 (1987).
[88]P. D. de Rèotier, P. Vulliet, A. Yaouanc *et al.*, Physica C **153-155**, 1541 (1988).
[89]S. G. Barsov, A. L. Getalov, V. P. Koptev *et al.*, Preprint No. 1447, Leningrad Institute Nuclear Physics [in Russian], Academy of Sciences of the USSR, Leningrad (1988).
[90]N. Nishida, H. Miyatake, S. Okuma *et al.*, Jpn. J. Appl. Phys. **27**, L94 (1988).
[91]D. T. Bezhitadze, I. P. Borovinskaya, Ya. Buryanek *et al.*, *Investigations of superconductors by the μ SR method at the phasotron of the Nuclear Physics Laboratory, Joint Institute for Nuclear Research* [in Russian], Preprint No. D14-89-455, Joint Institute for Nuclear Research, Dubna (1989).
[92]H. Maletta, P. Birrer, F. N. Gygax *et al.*, Proc. of the Fifth International Conference on μ SR–Oxford (1990), p. 55, will be published in Hyperfine Interactions **63–65** (1990).
[93]N. Nishida, H. Miyatake, D. Shimada *et al.*, Physica C **153-155**, 761 (1988).
[94]Y. Kuno, N. Nishida, H. Miyatake *et al.*, Phys. Rev. B **38**, 9276 (1988).
[95]E. Barth. P. Birrer, F. N. Gygax *et al.*, Physica C **153-155**, 767 (1988).
[96]B. Birrer, F. N. Gygax, B. Hitti *et al.*, Phys. Rev. B **39**, 11 449 (1989).
[97]W. K. Dawson, C. H. Halim, S. P. Weathersby *et al.*, Proc. of the Fifth International Conference on μ SR–Oxford (1990), p. 52, will be published in Hyperfine Interactions **63–65** (1990).
[98]D. W. Cooke, M. S. Jahan, R. S. Kwok *et al.*, Proc. of the Fifth International Conference on μ SR–Oxford (1990), p. 62, will be published in Hyperfine Interactions **63–65** (1990).
[99]H. Gluckler, Ch. Niedermayer, G. Nowitzke *et al.*, Proc. of the Fifth International Conference on μ SR–Oxford (1990), p. 58, will be published in Hyperfine Interactions **63–65** (1990).
[100]A. Schenck, P. Birrer, F. N. Gygax *et al.*, Proc. International Seminar on High-T_c Superconductivity, Joint Institute for Nuclear Research, Dubna (1989).
[101]A. Widerger, J. I. Budnick, B. Chamberland *et al.*, Physica C **153-155**, 168 (1988).
[102]C. Niedermayer, A. Golnick, E. Recknagle *et al.*, Phys. Rev. B **38**, 2836 (1988).
[103]Y. J. Uemura, W. J. Kossler, J. R. Kempton *et al.*, Physica C **153-155**, 769 (1988).
[104]Y. J. Uemura, W. J. Kossler, X. H. Yu *et al.*, Phys. Rev. Lett. **59**, 1045 (1987).
[105]J. I. Budnik, A. Golnick, Ch. Niedermayer *et al.*, Phys. Lett. A **124** 103 (1987).
[106]K. Sekizawa, Y. Takano, H. Takigami *et al.*, Jpn. J. Appl. Phys. **26**, L840 (1987).
[107]G. Aeppli, D. R. Harshman, D. Buttrey *et al.*, Physica C **153-155**, 1111.
[108]J. I. Budnick, B. Chamberland, D. P. Yang *et al.*, Europhys. Lett. **5**, 651 (1988).
[109]P. Gutsmiedl, G. Wolff, and K. Andres, Phys. Rev. B **36**, 4043 (1987).
[110]Y. Kitaoka, S. Hiramatsu, K. Ishida *et al.*, J. Phys. Soc. Jpn. **56**, 3024 (1987).
[111]E. Torikai, H. Kitazawa, K. Nagamine *et al.*, Proc. of the Fifth International Conference on μ SR–Oxford (1990), p. 63, will be published in Hyperfine Interactions **63–65** (1990).
[112]R. D. Renzi, G. Guidi, P. Carreta *et al.*, Phys. Lett. A **135**, 132 (1989).
[113]B. X. Yang, R. F. Kiefl, J. F. Brewer *et al.*, Phys. Rev. B **39**, 847 (1989).

Translated by J. R. Anderson